

Local Level Dynamic Random Partition Models for Changepoint Detection

Alice Giampino¹, Michele Guindani², Bernardo Nipoti¹, and Marina Vannucci³

¹Department of Economics, Management and Statistics, University of Milano-Bicocca, Milan,
Italy

²Department of Biostatistics, University of California Los Angeles, CA, U.S.A.

³Department of Statistics, Rice University, TX, U.S.A.

Abstract

Motivated by an increasing demand for models that can effectively describe features of complex multivariate time series, e.g. from sensor data in biomechanics, motion analysis, and sports science, we introduce a novel state-space modeling framework where the state equation encodes the evolution of latent partitions of the data over time. Building on the principles of dynamic linear models, our approach develops a random partition model capable of linking data partitions to previous ones over time, using a straightforward Markov structure that accounts for temporal persistence and facilitates changepoint detection. The selection of changepoints involves multiple dependent decisions, and we address this time-dependence by adopting a non-marginal false discovery rate control. This leads to a simple decision rule that ensures more stringent control of the false discovery rate compared to approaches that do not consider dependence. The method is efficiently implemented using a Gibbs sampling algorithm, leading to a straightforward approach compared to existing methods for dependent random partition models. Additionally, we show how the proposed method can be adapted to handle multi-view clustering scenarios. Simulation studies and the analysis of a human gesture phase dataset collected through various sensing technologies show the effectiveness of the method in clustering multivariate time series and detecting changepoints.

1 INTRODUCTION

Recently, there has been an increased demand for models that can effectively describe features of complex multivariate time series data. This surge in interest is particularly prominent in fields such as biomechanics, motion analysis, human-computer interaction, and sports science. Here, one of the goals is often to break down continuous human motion or activity into distinct phases and states. The insights derived from such analyses can then be used to improve sports performances and for

a deeper study of the complexity of human biomechanics, for example, to understand gait cycles, gesture phases, athletic movements, and even cognitive states. In the analysis of human gesture data, information is typically gathered through various sensing technologies, such as motion capture systems, accelerometers, or videos. These technologies yield rich datasets that capture the temporal patterns of human movements.

Let $\mathbf{Y}_1, \dots, \mathbf{Y}_T$ denote a multivariate time series, where each \mathbf{Y}_t is a n -dimensional vector, i.e., $\mathbf{Y}_t = \{Y_{1,t}, Y_{2,t}, \dots, Y_{n,t}\}$, observed on n units over T time points. To illustrate, consider our application in Section 5, where we examine scalar velocity data obtained from acceleration sensor units placed on the hands and wrists of a subject. Dynamic linear models (DLMs) are commonly employed for the analysis of time-series data due to their flexibility and adaptability in handling diverse situations (Petris et al., 2009). They define a class of state-space models and are characterized by a system of two equations: an observation equation, which describes the observed data as a linear combination of latent state variables with noise, and a state equation that describes how latent states evolve over time, thereby tracking the underlying dynamics of the system. We introduce our contribution by referring to a simple yet fundamental DLM, the *local level model*, which describes the observed data as composed of a level component plus random noise,

$$Y_{i,t} = \beta_{i,t} + \varepsilon_i, \quad (1)$$

where $\varepsilon_i \stackrel{\text{iid}}{\sim} \text{N}(0, \tau^2)$, with $\text{N}(\mu, \sigma^2)$ denoting the Normal distribution with mean μ and variance σ^2 . The vector $\boldsymbol{\beta}_t = (\beta_{1,t}, \dots, \beta_{n,t})$ represents the underlying level or trend of the time series at time t . In a typical local level model, the evolution of $\boldsymbol{\beta}_t$ over time is modeled as a random walk, i.e., the level at time t is predicted to be the same as the level at time $t - 1$, plus some random noise. If the variance of the random noise is small, this assumption implies smooth processes over time. Despite its simplicity, the local level model illustrates the fundamental characteristics of many time-series models, and will serve as a basic example throughout.

One of the main goals of our biometric data application is to study how measurements from different units cluster or group over time, as well as how these clusters evolve during an activity, to understand how different body parts cooperate during different stages of a gesture or movement. Furthermore, the detection of changepoints in the clustering of body parts between gesture stages can reveal important insights into the motion and inform gesture detection algorithms. In the Bayesian setting, Bayesian nonparametric (BNP) models are a popular choice for clustering dynamic behavior over time (Quintana et al., 2022). BNP models do not require the upfront specification of the number of clusters; instead, they allow for posterior inference on cluster allocations directly from the data. Existing BNP approaches for clustering time series data vary in terms of motivation, application, and how time-dependence is introduced. For example, some approaches build on the stick-breaking

representation of the Dirichlet Process (Ferguson, 1973; Sethuraman, 1994). In this context, Antoniano-Villalobos and Walker (2016) have developed a stationary Markov model where both the transition and stationary densities are nonparametric infinite mixture models. Nieto-Barajas and Contreras-Cristán (2014) have clustered temporal data while considering several features typical of time series data (e.g., trends and seasonality). BNP autoregressive model are discussed in Kalli and Griffin (2018), De Iorio et al. (2019), DeYoreo and Kottas (2018), and Beraha et al. (2022), among others. Alternatively, other authors have explored generalizations of the Pólya urn scheme of Blackwell et al. (1973), see, e.g. Caron et al. (2007), Caron et al. (2017) and Cassese et al. (2019).

All methods mentioned above identify clusters based on the values of associated parameters, e.g. the latent variables $\beta_{i,t}$ in the illustrative local level model (1). These models can potentially detect changepoints in the partitions of the data over time if, for instance, two data points assume a common value at times t and $t+1$ but that value changes significantly between time points. This occurs because model-based clustering with Bayesian nonparametric models essentially relies on specifying a mixture model that depends on a discrete random mixing measure. The probabilistic distribution over random partitions is essentially a by-product of this mixture setup; in essence, clusters in a mixture model are identified based on the values of the process' atoms. We illustrate this point in Figure 1 in the case of clustering of sensors, where the grouping may not depend on the intensity of the values but rather on the dependences of the movements.

A solution to address this challenge involves directly modeling the sequence of random partitions. In this context, Page et al. (2022) introduced a dependent random partition model (Hartigan, 1990; Barry and Hartigan, 1992) that incorporates auxiliary variables that determine whether a unit, for which the cluster allocation at time $t-1$ has been determined, should be considered for possible cluster reallocation at time t . As a result, a change of partitions over time is obtained as a by-product of individual clustering allocations. This may lead to a high number of cluster configurations and may hinder the identification of partition changepoints through time, which is crucial, for instance, in identifying gesture phases. Quinlan et al. (2022) presented a method that aims to correlate partitions with the detection of changepoints in multivariate time series in the context of contagion phenomena. However, following Martinez and Mena (2014), they specify only a single unique partition of contiguous clusters for each time series. The focus of their model is on multivariate changepoint detection rather than data partitioning, with changepoints occurring at different time points for each time series. In this paper, we propose viewing the evolution of partitions over time as latent partition-based states within a state-space model. Our approach develops a random partition model (RPM) capable of linking the partition of data points to previous partitions over time, using a straightforward Markov structure to model these changes. The approach builds upon the principles of DLMS but extends them to incorporate latent state equations now operating within the partition context and time evolution

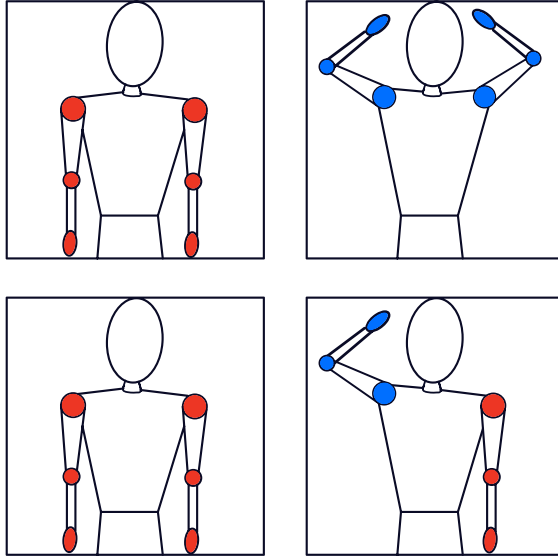


Figure 1: Example of sensors’ clusters at two-time points (left, right). The colors identify the clusters. Top image: the arms remain together in the left and right picture; in mixture-based clustering models the sensors’ measurements (e.g., scalar velocity) may lead to a change in the cluster label assigned to the sensors, although the partition remains the same. Bottom image: the movements, captured by a different scalar velocity measured across sensors, create two different partitions of the sensors.

defined by the partitions themselves. Therefore, while in the analysis of time series data, it is common to identify sudden changes in the observed values of a stochastic process as a changepoint, in this paper, we refer to a changepoint as a change in a latent partition of units. More specifically, we employ a Markov-dependent structure, where the partition at time t , denoted as π_t , is modeled conditionally on the partition at time $t - 1$, accounting for temporal persistence and enabling changepoint detection. The selection of changepoints at each time point t is driven by a mixture that chooses between one of two partitions. At any given time, the chosen partition can either remain the same as the one at the previous time point or be sampled from a flexible and general random partition model. In the presence of a changepoint, the partition at time t becomes independent of the partition at time $t - 1$. We demonstrate that, based on our construction, the random partitions π_t , for $t = 1, \dots, T$, are marginally identically distributed, with the marginal distribution that can be specified so to ensure tractability. Unlike the existing Bayesian nonparametric models cited above, our clustering approach does not directly rely on the values of parameters, such as the $\beta_{i,t}$ ’s in equation (1). Instead, we directly treat dependent random partition allocations as latent structures that drive the dynamics of the observations. In contrast to the dependent random partition model proposed by Page et al. (2022), we jointly consider all the units when identifying changepoints, taking into account the multivariable nature of the dependent partitions.

For posterior inference, our approach relies on the efficiency of a Gibbs sampling algorithm, offering a straightforward implementation compared to existing methods for dependent random partition models. The selection of changepoints involves dependent multiple decisions, and we propose accounting for this time-dependence by adapting the decision-theoretic approach of [Chandra and Bhattacharya \(2019\)](#) in defining the error and non-error terms of the decision loss function. The resulting procedure establishes a simple decision rule that ensures more stringent control of the false discovery rate compared to an approach that does not consider dependence.

Recent methods have been proposed for multiview clustering that allow for dependence between several experimental conditions or features. For example, [Franzolini et al. \(2023\)](#) employ a conditional partially exchangeable model to induce dependence between clustering configurations of the same subjects across different features. Similarly, [Dombowsky and Dunson \(2023\)](#) develop a nonparametric prior that generates dependent random distributions by centering a Dirichlet process on a random product measure, with a single parameter controlling the dependence. Our approach can also be adapted for multi-view clustering scenarios. By incorporating a latent-state representation of the partitions, our framework builds a hierarchical model that effectively captures the dependence between partitions, describing changes across different groups or experimental conditions. Additionally, we show that the dependence between the partitions generated by the hierarchical model for multiview clustering in [Dombowsky and Dunson \(2023\)](#) coincides with that one of a reparametrization of our prior specification. Finally, we should note that while constructing the prior distribution for the partition bears some resemblance to the use of spike-and-slab priors for variable selection ([Tadesse and Vannucci, 2021](#)), dealing with partitions introduces additional complexity in the motivation, modeling and computation.

The article is organized as follows: in [Section 2](#), we present our model and discuss its main properties. [Section 2.2](#) discusses the alternative multiview formulation of our model. In [Section 3](#) we cover posterior inference, including computational methods and decision theory-based changepoint detection. In [Section 4](#) we describe two simulation studies that highlight the key aspects of our model. In [Section 5](#), we present an application to the analysis of human gesture data, and finally, in [Section 6](#), we provide concluding remarks and outline future directions. Proofs and additional details on computations and illustrations are available in the Supplementary Material.

2 LOCAL LEVEL DYNAMIC PARTITION MODEL

We describe the key features of the dynamic partition model we propose, a local level dynamic partition model (LLDPM) taking model [\(1\)](#) as reference. More specifically, we assume that for each unit i , with

$i = 1, \dots, n$, the observations are generated from some general likelihood (observation equation) as

$$Y_{i,t} \mid \beta_{i,t} \stackrel{\text{ind}}{\sim} p(y_{i,t} \mid \beta_{i,t}), \quad (2)$$

for $t = 1, \dots, T$ and $i = 1, \dots, n$. Throughout this work, we consider a Gaussian kernel with mean $\beta_{i,t}$ and variance τ^2 . However, it is possible to extend this construction to other kernels. The dynamics of the latent state equation are characterized in terms of time-varying partitions of the n units over time. In order to describe such dynamics, we introduce a dependent RPM that models temporal dependence in terms of sequences of partitions by considering an auxiliary variable determining whether the partition at time $t-1$ will be revised for possible reallocation of the units at time t , for $t = 1, \dots, T$. More specifically, we introduce a binary *changepoint* auxiliary variable $\gamma_t \in \{0, 1\}$, to detect changes in the partitions of the n units from time $t-1$ to time t . We use $|\cdot|$ to indicate the cardinality of a set, and thus denote the number of blocks composing a partition π_t of n units as $|\pi_t|$. Further, we let $\pi_t = \{C_{1,t}, \dots, C_{|\pi_t|,t}\}$, where, for each $j = 1, \dots, |\pi_t|$, the set $C_{j,t}$ consists of the indices corresponding to the statistical units assigned to the j -th cluster according to π_t . Thus, given a partition π_{t-1} at time $t-1$, we assume a *partition-based state equation* characterized as a mixture over two partition models, corresponding to the case of conditionally independent and identical random partitions at subsequent time points. Namely,

$$\begin{aligned} \pi_t \mid \boldsymbol{\pi}_{1:(t-1)}, \boldsymbol{\gamma}_{2:t} &\sim (1 - \gamma_t) \delta_{\pi_{t-1}}(\pi_t) + \gamma_t p^*(\pi_t), \quad t = 2, \dots, T \\ \pi_1 &\sim p^*(\pi_1) \end{aligned} \quad (3)$$

where $\boldsymbol{\pi}_{1:(t-1)} = (\pi_1, \dots, \pi_{t-1})$ is the vector of previously recorded partitions, $\boldsymbol{\gamma}_{2:t} = (\gamma_2, \dots, \gamma_t)$ indicates the vector of changepoints, and $p^*(\cdot)$ is a distribution over the space of partitions of n units, henceforth referred to as the *base partition distribution*. In addition, we make an assumption on the distribution of the changepoints γ_t in (3), that is

$$\gamma_t \stackrel{\text{ind}}{\sim} \text{Bern}(\eta_t), \quad t = 2, \dots, T. \quad (4)$$

The probability of a changepoint, η_t , can then be seen as a dependence parameter, with the extreme case $\eta_t = 0$ leading to almost surely identical partitions at time $t-1$ and t . In the remaining of the work, we will call *partition state model* (PSM) the model for the random partitions $\boldsymbol{\pi}_{1:T}$ defined through (3) and (4). Alternative partition-based state equations, and thus partition state models, can potentially be defined, to describe more complex forms of temporal dependence. See Section 6 for more discussion. The LLDPM is thus obtained by combining the PSM with (2), where, as standard in Bayesian nonparametric models, we assume that at each time point $t = 1, \dots, T$, the values of the parameters $\beta_{i,t}$, with $i = 1, \dots, n$, coincide within a cluster, although the specific values could differ at

different times. If we let $\{\beta_{1,t}^*, \dots, \beta_{|\pi_t|,t}^*\}$ denote the set of distinct values in β_t , such assumption on β_t can be formalized as

$$\beta_t \mid \pi_t \sim \prod_{j=1}^{|\pi_t|} P_0(\beta_{j,t}^*), \quad (5)$$

for some base probability distribution $P_0(\cdot)$.

2.1 PRIOR PROPERTIES OF THE PSM

We assume that the base partition distribution $p^*(\cdot)$ is the one implied by the class of Gibbs-type priors (De Blasi et al., 2013). Distributions over partitions are conveniently described through the exchangeable partition probability function (EPPF), a simple way to define probabilistic partition models based on the number and sizes of blocks, independently of the object labels. De Blasi et al. (2013) show that exchangeable product partition models with probability of each partition depending only on the cardinality of each cluster coincide with the family of Gibbs-type priors. A Gibbs-type EPPF has the following form,

$$\mathbb{P}_\theta [\pi_t = \{C_{1,t}, \dots, C_{|\pi_t|,t}\}] = V_{n,|\pi_t|} \prod_{j=1}^{|\pi_t|} \frac{\Gamma(|C_{j,t}| - \sigma)}{\Gamma(1 - \sigma)}, \quad (6)$$

with $-\infty \leq \sigma < 1$, and where, for any $n \geq 1$ and any $k = 1, \dots, n$, the set of non-negative weights $V_{n,k}$ satisfies the following recursive equation $V_{n,k} = (n - \sigma k)V_{n+1,k} + V_{n+1,k+1}$, and is such that $V_{1,1} = 1$. Notable elements of the class of Gibbs-type priors are the Dirichlet and the Pitman-Yor processes (Ferguson, 1973; Pitman and Yor, 1997), mixtures of symmetric Dirichlet distributions (Gnedin and Pitman, 2005), the normalized inverse Gaussian processes (Lijoi et al., 2005) and the normalized generalized gamma process (Lijoi et al., 2007). Throughout the paper, as a running example for the base partition distribution $p^*(\cdot)$, we will consider the Chinese restaurant process (CRP, Pitman, 2002) with concentration parameter $\theta > 0$, denoted as $p_{\text{CRP}}(\cdot)$, which can be obtained as the distribution on the partitions implied by the Dirichlet process. The corresponding EPPF is readily obtained by setting $\sigma = 0$ and $V_{n,|\pi_t|} = \theta^{|\pi_t|} / (\theta)_n$ in (6), where $(\theta)_n = \theta(\theta + 1) \cdots (\theta + n - 1)$ denotes the ascending factorial. For each specification within the class of Gibbs-type priors, the weights $V_{n,k}$ can be computed recursively or estimated via Monte Carlo (Arbel et al., 2017).

We study the temporal dependence of random partitions implied by the proposed PSM. We begin by observing that, once the changepoints $\gamma_{2:T}$ are marginalized out, the distribution of $\pi_{1:T}$ implied

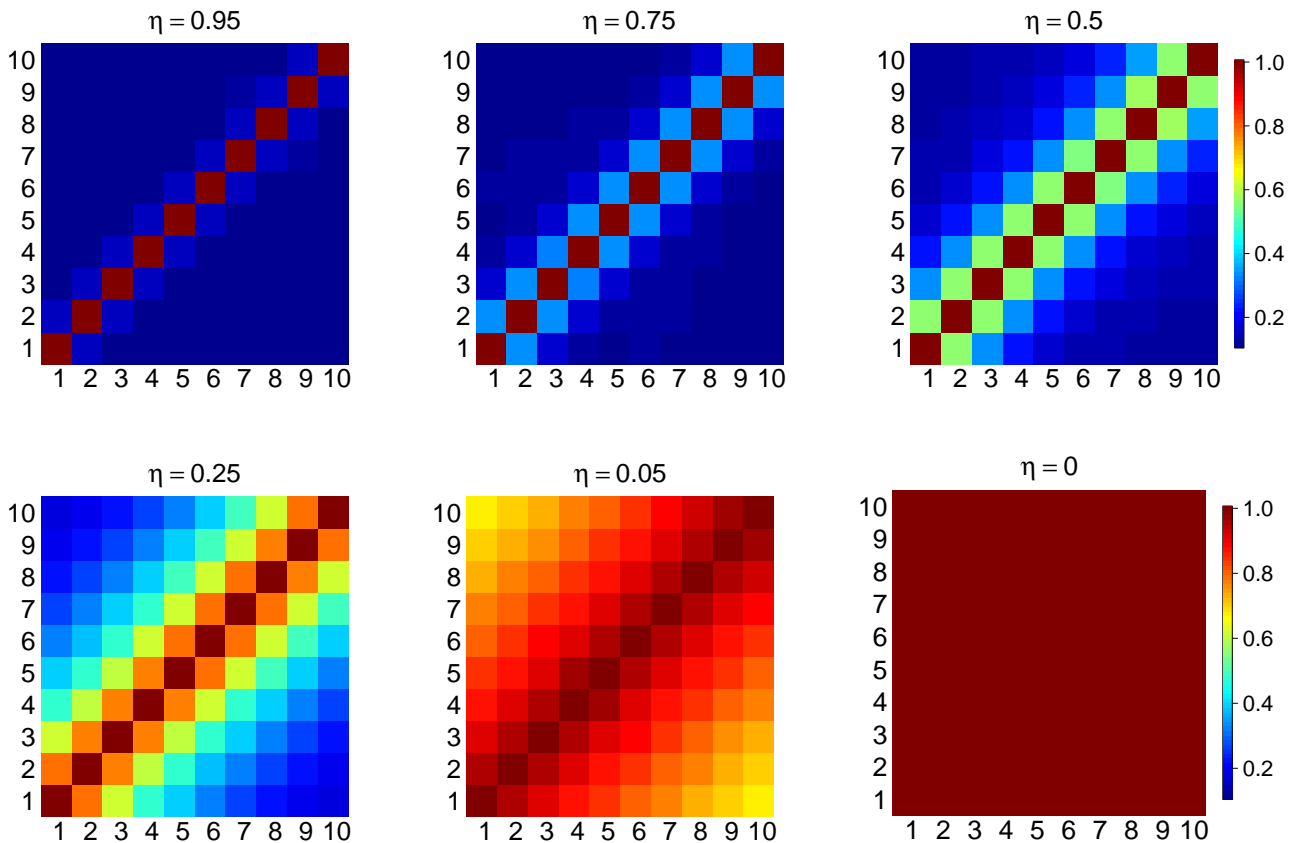


Figure 2: Average lagged ARI for the pairwise comparison of $T = 10$ random partitions $\pi_{1:T}$ modeled according to the proposed PSM with $p^*(\cdot) = p_{\text{CRP}}(\cdot)$. From top-left panel to bottom-right panel, η ranges in $\{0.95, 0.75, 0.5, 0.25, 0.05, 0\}$. For each matrix, the pixel in position (i, j) refers to the comparison of π_i and π_j . For each value of η , values of the lagged ARI are averaged over a sample of 10,000 partitions. The temporal dependence increases as the temporal dependence parameter η decreases.

by the PSM is given by

$$\pi_{1:T} \sim p^*(\pi_1) \prod_{t=2}^T [(1 - \eta_t) \delta_{\pi_{t-1}}(\pi_t) + \eta_t p^*(\pi_t)].$$

Figure 2 shows the average Adjusted Rand Index (ARI) (Rand, 1971) between time-lagged partitions, similarly to Figure 2 in Page et al. (2022), assuming $T = 10$, for several values of the temporal dependence parameter, $\eta_t = \eta \in \{0, 0.05, 0.25, 0.5, 0.75, 0.95\}$, $t = 2, \dots, T$. For each value of η and for each pair of times $t_1, t_2 \in \{1, \dots, T\}$, the average lagged ARI, comparing π_{t_1} and π_{t_2} , is computed over 10,000 partitions simulated from the proposed PSM with $p^*(\cdot) = p_{\text{CRP}}(\cdot)$. Figure 2 shows increasing temporal dependence of the lagged partitions as η decreases. The dependence across partitions at different times can be investigated more formally by computing the expected Rand Index (ERI). For two random partitions π_{t_1} and π_{t_2} , the Rand Index is a random variable defined as

$R(\pi_{t_1}, \pi_{t_2}) = (A_{t_1, t_2} + B_{t_1, t_2}) / \binom{n}{2}$, where A_{t_1, t_2} is the number of pairs of observations that are in the same cluster in both partitions, and B_{t_1, t_2} is the number of pairs that are in different clusters in both partitions. The corresponding ERI, φ_{t_1, t_2} , is then defined as

$$\varphi_{t_1, t_2} = \mathbb{E}[R(\pi_{t_1}, \pi_{t_2})] = \sum_{\pi_{t_1}, \pi_{t_2} \in \mathcal{P}} R(\pi_{t_1}, \pi_{t_2}) p(\pi_{t_1}, \pi_{t_2}),$$

where \mathcal{P} indicates the space of all possible partitions of n elements, and $p(\pi_{t_1}, \pi_{t_2})$ stands for the joint distribution of the random partitions π_{t_1} and π_{t_2} . We obtain the ERI for two random partitions whose joint distribution is defined through the proposed PSM and the base partition distribution $p^*(\cdot)$ implied by a Gibbs-type prior. We first focus on partitions at subsequent time points, that is $t_2 = t_1 + 1$, and then consider the more general case $t_1 < t_2$.

Proposition 1. *Suppose $t_2 = t_1 + 1$ and $\eta_{t_1} = \eta_{t_2} = \eta$. Let $p^*(\cdot)$ be the distribution over partitions implied by a Gibbs-type prior. Then the ERI for two random partitions π_{t_1} and π_{t_2} modeled according to a PSM is given by*

$$\varphi_{t_1, t_2} = 1 - 2V_{2,2}(1 - V_{2,2})\eta. \quad (7)$$

The ERI is thus a decreasing function of the dependence parameter value η . Moreover, as $\eta \rightarrow 0$, the ERI approaches one, its maximum value, indicating that the partitions are identical. Conversely, as $\eta \rightarrow 1$, the ERI converges to $1 - 2V_{2,2}(1 - V_{2,2})$, which is the ERI of two independent and identically distributed partitions with distribution implied by a Gibbs-type prior. As a matter of fact, the expression in (7) can be rewritten as a convex linear combination of the two limiting cases, that is

$$\varphi_{t_1, t_2} = (1 - \eta) + [1 - 2V_{2,2}(1 - V_{2,2})]\eta.$$

When $p^*(\cdot) = p_{\text{CRP}}(\cdot)$, the ERI for two random partitions at subsequent times modeled according to the proposed PSM is obtained by substituting the appropriate specification of $V_{2,2}$ in Proposition 1, which leads to the following corollary.

Corollary 1. *Suppose $t_2 = t_1 + 1$ and $\eta_{t_1} = \eta_{t_2} = \eta$ and let $p^*(\cdot) = p_{\text{CRP}}(\cdot)$. Then the ERI for two random partitions π_{t_1} and π_{t_2} modeled according to a PSM is given by*

$$\varphi_{t_1, t_2} = 1 - \frac{2\theta}{(\theta + 1)^2}\eta. \quad (8)$$

The expression for the ERI in (8) coincides, up to a reparametrization of the dependence parameter η , with an analogous result derived in [Dombowsky and Dunson \(2023\)](#). Interestingly, the ERI approaches one both when $\theta \rightarrow 0$ and when $\theta \rightarrow \infty$. This behavior is not surprising as, when θ approaches zero, the distribution of both random partitions tend to assign mass one to the partition with only one

block. Similarly, when θ increases, the two distributions accumulate mass at the partition composed of n blocks of size one. In both cases, the two random partitions tend to take the same configuration, regardless of the value taken by the dependence parameter η . Also in this case, (8) can be written as a convex linear combination of the ERI of two identical random partitions, that is one, and the ERI of two independent random partitions both distributed as a Chinese restaurant process, that is $(\theta^2 + 1)/(\theta + 1)^2$. The next proposition describes how the dependence between two lagged random partitions modeled through the proposed PSM changes as a function of the lag $t_2 - t_1$.

Proposition 2. *Suppose $t_1 < t_2$ and let $\eta_{t_1} = \eta_{t_2} = \eta$. Let $p^*(\cdot)$ be the distribution over partitions implied by a Gibbs-type prior. Then the ERI for two random partitions π_{t_1} and π_{t_2} modeled according to a PSM is given by*

$$\varphi_{t_1, t_2} = 1 - 2V_{2,2}(1 - V_{2,2}) [1 - (1 - \eta)^{t_2 - t_1}].$$

The ERI is thus a decreasing function of the time lag $t_2 - t_1$. Furthermore, regardless of the value of the dependence parameter η , the limit of φ_{t_1, t_2} as $(t_2 - t_1) \rightarrow \infty$ tends towards the ERI of two independent random partitions with identical distribution implied by a Gibbs-type prior. The next corollary specializes the previous result to the case $p^*(\cdot) = p_{CRP}(\cdot)$.

Corollary 2. *Suppose $t_1 < t_2$ and let $\eta_{t_1} = \eta_{t_2} = \eta$. If $p^*(\cdot) = p_{CRP}(\cdot)$, then the ERI for two random partitions π_{t_1} and π_{t_2} modeled according to a PSM is given by*

$$\varphi_{t_1, t_2} = 1 - \frac{2\theta}{(\theta + 1)^2} [1 - (1 - \eta)^{t_2 - t_1}]. \quad (9)$$

We next explore the marginal distribution of the components of $\boldsymbol{\pi}_{1:T}$, under the assumption of a PSM for $\boldsymbol{\pi}_{1:T}$, with generic base partition distribution $p^*(\cdot)$. We prove that at each time t , the marginal distribution of the random partition π_t is the same as that of the base partition distribution $p^*(\cdot)$, for $t = 2, \dots, T$. Thus, although the PSM explicitly models the evolution of the random partitions $\boldsymbol{\pi}_{1:T}$ over time, the components of $\boldsymbol{\pi}_{1:T}$ are marginally identically distributed according to $p^*(\cdot)$. Importantly, this result holds regardless of the specific distribution $p^*(\cdot)$, which therefore could be specified also outside the class of Gibbs-type priors considered here.

Proposition 3. *Let $\boldsymbol{\pi}_{1:T}$ be modeled according to a PSM. Then, for every $t = 1, \dots, T$, the marginal distribution of the random partition π_t coincides with the base partition distribution $p^*(\cdot)$.*

2.2 MULTIVIEW CLUSTERING REPRESENTATION OF THE LLDPM

In many real-world applications, data can be collected from various sources or represented using different feature sets, creating multiple views of the same underlying entities. In this section, we present an alternative representation of our model that establishes a hierarchical structure in the dependence

of partitions, deviating from the assumption of temporally dependent partitions where each partition depends on the previous one. This hierarchical representation effectively describes changes in the partition across different groups or experimental conditions, offering a flexible and interpretable approach to modeling and understanding partition relationships. Such representation exemplifies a multiview clustering model, bearing close connections to the partition introduced by [Dombowsky and Dunson \(2023\)](#) and related to the multiview representation in [Franzolini et al. \(2023\)](#). As noted below (8), the same expected dependence between partitions induced by the hierarchical model for multiview clustering in [Dombowsky and Dunson \(2023\)](#) can be achieved by our model by reparametrizing the dependence parameter η . In their prior specification, dependence is introduced through the concentration parameter of a Dirichlet process, which determines the tendency of data points to form distinct groups. The main difference between our model and theirs lies in the way the dependence is induced. While their models specify a dependence structure on the atoms within a hierarchical model on a product space, our model introduces dependence directly at the level of partitions, providing a more streamlined approach to modeling partition relationships.

We begin by examining the joint distribution of two subsequent random partitions in the PSM we proposed, where T can now be interpreted as the number of different views, groups or experimental conditions, depending on the context of the application. Without loss of generality, we consider the case where $T = 2$ and thus focus on the joint distribution of π_1 and π_2 , as implied by the PSM, which is

$$\boldsymbol{\pi}_{1:2} \sim p^*(\pi_1) [(1 - \eta)\delta_{\pi_1}(\pi_2) + \eta p^*(\pi_2)], \quad (10)$$

where η is used to denote the dependence parameter. This distribution can be obtained as the marginal distribution of a hierarchical random partition model. To see this, we consider a third random partition distributed according to the base partition distribution, namely

$$\tilde{\pi} \sim p^*(\tilde{\pi}). \quad (11)$$

In this alternative representation, $\tilde{\pi}$ serves as a common parent partition for both π_1 and π_2 , by assuming the following generative model for π_1 and π_2 ,

$$\pi_t \mid \tilde{\pi}, \tilde{\gamma}_1, \tilde{\gamma}_2 \stackrel{\text{ind}}{\sim} (1 - \tilde{\gamma}_t) \delta_{\tilde{\pi}}(\pi_t) + \tilde{\gamma}_t p^*(\pi_t), \quad t = 1, 2, \quad (12)$$

where $\tilde{\gamma}_t \stackrel{\text{iid}}{\sim} \text{Bern}(\tilde{\eta})$, $t = 1, 2$, controlling the degree to which π_1 and π_2 can differ from the parent partition $\tilde{\pi}$. A higher value of $\tilde{\eta}$ increases the chances of π_t being different from $\tilde{\pi}$, allowing for more flexibility and individual variations in the partition structure. Conversely, a lower value of $\tilde{\eta}$ makes

it more likely that π_t will follow the same partition structure as $\tilde{\pi}$, enforcing a stronger dependence between the two. Note that, in model (11)–(12), the distribution of π_2 is independent of that of π_1 , given the partition $\tilde{\pi}$. The joint distribution of the random partitions π_1 and π_2 , the common parent partition $\tilde{\pi}$, and the dependence variables $(\tilde{\gamma}_1, \tilde{\gamma}_2)$, here denoted by $p(\boldsymbol{\pi}_{1:2}, \tilde{\pi}, \tilde{\gamma}_1, \tilde{\gamma}_2)$, can thus be written as

$$p(\boldsymbol{\pi}_{1:2}, \tilde{\pi}, \tilde{\gamma}_1, \tilde{\gamma}_2) \sim p^*(\tilde{\pi}) \left\{ \prod_{t=1}^2 [(1 - \tilde{\gamma}_t) \delta_{\tilde{\pi}}(\pi_t) + \tilde{\gamma}_t p^*(\pi_t)] \tilde{\eta}^{\tilde{\gamma}_t} (1 - \tilde{\eta})^{1 - \tilde{\gamma}_t} \right\}.$$

Hence, the distribution of π_1 and π_2 is obtained by marginalizing the last expression with respect to $\tilde{\pi}$ and $(\tilde{\gamma}_1, \tilde{\gamma}_2)$, which gives (10), provided that $\tilde{\eta} = 1 - \sqrt{1 - \eta}$.

Hence, the local level partition model’s joint distribution on the partitions can be viewed as a special case of a hierarchical partition model, when considered marginally. This representation highlights the connection between the time-varying formulation of the PSM, as specified through (3)–(4), and an exchangeable model on the partitions, under the assumptions of identical marginal distributions of the partitions, $p^*(\pi_t)$, and equal Bernoulli probabilities $\tilde{\eta}$ across groups. This hierarchical representation can be extended to accommodate $T \geq 2$ groups, with one parent random partition driving the distribution of T identically distributed random partitions. Moreover, the assumption of a common Bernoulli probability $\tilde{\eta}$ across groups can be relaxed to accommodate for group-specific parameters $\tilde{\eta}_t$, with $t = 1, \dots, T$. Expressing the local level partition model as a hierarchical model provides an alternative viewpoint to appreciate its flexibility in capturing both similarities and dissimilarities among the partitions. The hierarchical structure allows for the sharing of information across groups while still accommodating individual variations in the partition structures.

3 POSTERIOR INFERENCE

Posterior inference for the parameters of the LLDPM is carried out using a Markov chain Monte Carlo (MCMC) algorithm and, more specifically, a Gibbs sampling scheme (Neal, 2000). For computational convenience, we marginalize with respect to the local level parameters $\boldsymbol{\beta}_t$, thus introducing, for any $t = 1, \dots, T$, the conditional distribution of the observations \mathbf{Y}_t , given the partition π_t , namely

$$p(\mathbf{Y}_t | \pi_t) = \prod_{j=1}^{|\pi_t|} \int \prod_{i \in C_{j,t}} p(y_{i,t} | \beta_{j,t}^*) P_0(d\beta_{j,t}^*).$$

The algorithm comprises three main steps, with particular attention needed for jointly updating the random partition π_t and the changepoint γ_t from their full conditional distribution. The updates also include the dependence parameters η_t , for which we specify a hyperprior distribution as $\eta_t \stackrel{\text{iid}}{\sim} \text{Beta}(a, b)$.

We briefly describe the updates of the model parameters at a generic iteration. For simplicity, we do not introduce explicit notation to indicate at which iteration random quantities have been updated. Instead, the full conditional distributions for each update should be understood as being conditional on the most up-to-date values of the random quantities involved in the algorithm. The algorithm is presented for the case $p^*(\cdot) = p_{\text{CRP}}(\cdot)$. Extending it to other base partition distributions is conceptually straightforward. Additional details on the posterior distributions and our implementation can be found in Section B of the Supplementary Material.

1) *Joint update of (π_t, γ_t) .* For any $t = 1, \dots, T$, we follow a two-step procedure.

1.1) We update π_t from its full conditional distribution, computed after marginalizing γ_t out.

Namely

$$p(\pi_t | \dots) \propto \left[(1 - \eta_t) \delta_{\pi_{t-1}}(\pi_t) + \eta_t p_{\text{CRP}}(\pi_t) \right] \times \left[(1 - \gamma_{t+1}) \delta_{\pi_{t+1}}(\pi_t) + \gamma_{t+1} p_{\text{CRP}}(\pi_{t+1}) \right] p(\mathbf{Y}_t | \pi_t). \quad (13)$$

The form of the full conditional in (13) highlights that the update of π_t depends also on γ_{t+1} , the changepoint variable at the subsequent time step. We then distinguish between two cases:

1.1a) If $\gamma_{t+1} = 1$, indicating a changepoint at time $t + 1$, then no information about the distribution of π_t is borrowed from the subsequent time step. Thus, the full conditional of π_t boils down to the following mixture:

$$p(\pi_t | \gamma_{t+1} = 1, \dots) \propto (1 - \eta_t) p(\mathbf{Y}_t | \pi_{t-1}) \delta_{\pi_{t-1}}(\pi_t) + \eta_t p_{\text{CRP}}(\pi_t) p(\mathbf{Y}_t | \pi_t).$$

That is, π_t coincides with π_{t-1} with probability proportional to $(1 - \eta_t)p(\mathbf{Y}_t | \pi_{t-1})$. Alternatively, it is generated as a random draw of a new partition from a random partition model with distribution proportional to $p_{\text{CRP}}(\pi_t)p(\mathbf{Y}_t | \pi_t)$. The probability of choosing this mixture component is proportional to $\eta_t g_t$, where

$$g_t = \sum_{\pi_t \in \mathcal{P}} p_{\text{CRP}}(\pi_t) p(\mathbf{Y}_t | \pi_t) \quad (14)$$

is the marginal likelihood specific to time t . Later in the section we discuss how to evaluate g_t and how to sample from a distribution proportional to $p_{\text{CRP}}(\pi_t)p(\mathbf{Y}_t | \pi_t)$.

1.1b) If $\gamma_{t+1} = 0$, indicating there is not a changepoint at time $t + 1$, then the full conditional distribution of π_t is degenerate at π_{t+1} . Thus we simply set π_t equal to the current value of π_{t+1} .

1.2) We update the changepoint variable γ_t from its full conditional distribution, thus conditioning on the value of π_t as updated in step 1.1. This is equivalent with sampling a Bernoulli

random variable with probability of success

$$\Pr(\gamma_t = 1 \mid \dots) = \frac{\eta_t p_{\text{CRP}}(\pi_t)}{\eta_t p_{\text{CRP}}(\pi_t) + (1 - \eta_t) \delta_{\pi_{t-1}}(\pi_t)}.$$

We observe that, if $\pi_t \neq \pi_{t-1}$, then $\gamma_t = 1$ almost surely.

- 2) *Update of η_t .* For any $t = 1, \dots, T$, we update η_t from its full conditional distribution, which is given by

$$\eta_t \mid \dots \stackrel{\text{ind}}{\sim} \text{Beta}(a + \gamma_t, b + 1 - \gamma_t).$$

- 3) *Reshuffling step.* Conditionally on $\gamma_{2:T}$, we update the partitions $\pi_{1:T}$ using a sampling importance resampling step, as described in Section B.2 of the Supplementary Material.

Step 1.1a highlights the computational challenges that arise when implementing our PSM. Although the partition-based state equation (3) has the same mixture representation that characterizes tractable priors, such as the spike-and-slab prior commonly used for variable selection, working with random partitions makes computations more complex. The time-specific marginal likelihood (14) is estimated via Monte Carlo, a step that, conveniently, must be performed only once, prior to running the Gibbs sampler. Section B.1 in the Supplementary Material provides further details on how this step can be made efficient. Step 1.1a also involves sampling from a distribution proportional to $p_{\text{CRP}}(\pi_t)p(\mathbf{Y}_t \mid \pi_t)$, for every $t = 1, \dots, T$. We propose implementing an auxiliary MCMC run prior to initializing the primary MCMC algorithm for model fitting. In this preliminary run, we fit an independent CRP model at each time point. We then save all the partitions generated throughout the MCMC iterations, creating, for each $t = 1, \dots, T$, a catalogue \mathcal{S}_t of realizations from the posterior distribution of π_t given \mathbf{Y}_t . The size of these catalogues can be arbitrarily large. To sample a new partition from a distribution proportional to $p_{\text{CRP}}(\pi_t)p(\mathbf{Y}_t \mid \pi_t)$, we refer to the relevant catalogue of realized partitions from the auxiliary MCMC run, randomly selecting a new partition from \mathcal{S}_t , for $t = 1, \dots, T$. This strategy is crucial for making the resulting MCMC algorithm efficient and capable of handling observations recorded over a large number of time points T . For instance, this is the case in the application presented in Section 5, where $T = 349$.

3.1 CHANGEPOINT DETECTION

Changepoint detection inherently involves making multiple comparisons, since the decisions are temporally dependent. To address this multi-comparison problem, we use a compound decision-theoretic approach to detect the presence of a changepoint, which is based on a loss function that takes simultaneously into account the sequence of decisions, and it is defined as a linear combination of measures of the false positive and true positive (or, alternatively, false negative) decisions (Sun and Cai, 2007).

In a Bayesian context, Müller et al. (2004) and Müller et al. (2006) have demonstrated that, under the assumption of both independent hypotheses and independent (marginal) loss functions, the optimal approach for minimizing the resulting posterior expected loss involves thresholding the posterior probabilities of the changepoint (PPC_t), $\Pr(\gamma_t = 1 \mid \mathbf{Y}_1, \dots, \mathbf{Y}_T)$, for $t = 1, \dots, T$, as estimated from the MCMC output. However, such a procedure does not inherently control for a given false discovery rate (FDR) unless such control is explicitly accounted for. That is, we need to determine the optimal threshold in order to control the FDR at a specific desired level, say ζ . More in detail, we consider the Bayesian FDR (Newton et al., 2004),

$$\text{BFDR}_m(h) = \frac{\sum_{t=1}^T (1 - \text{PPC}_t) \mathbb{1}_{\{\text{PPC}_t > h\}}}{\max\left(\sum_{t=1}^T \mathbb{1}_{\{\text{PPC}_t > h\}}, 1\right)}, \quad (15)$$

where h is the chosen threshold and $\mathbb{1}_{\{\text{PPC}_t > h\}}$ is an indicator function such that $\mathbb{1}_{\{\text{PPC}_t > h\}} = 1$ if $\text{PPC}_t > h$, and 0 otherwise. The optimal threshold h^* corresponds to the minimum value of h that ensures that the BFDR_m is less than ζ . In formulas, $h^* = \min\{h : \text{BFDR}_m(h) \leq \zeta\}$. The previous testing procedure can be classified as a *marginal* approach (hence, the subscript in BFDR_m) since it fails to consider existing dependences either among hypotheses or in the decisions themselves. Sun et al. (2015) extended this framework to the spatial setting, explicitly taking into account dependences among the hypotheses, as induced by a spatial model. More recently, Chandra and Bhattacharya (2019) introduced *non-marginal* loss functions and non-marginal decision rules that directly account for dependences in the decision-making process. Their procedure incorporates additional information about dependences among tests into the definition of error and non-error terms for subgroups of hypotheses. Specifically, the approach penalizes each hypothesis based on incorrect decisions related to other dependent tests, thus defining a compound loss where decisions about dependent tests are interrelated. We adapt their framework to our case. For each time point $t = 1, \dots, T$, the detection of a changepoint at t is related to the probability of a changepoint at times $t - 1$ and $t + 1$. That is, the null hypothesis $H_{0,t}$, i.e. no changepoint at time t , is assessed with respect to the related decisions at times $t - 1$ and $t + 1$. Considering this set of dependent hypotheses together is crucial, since, for example, a false changepoint detection at time $t - 1$ may induce a false changepoint detection at time t , even if the null hypothesis is true at both times. We let d_t represent the decision at time t , i.e., $d_t = 1$ if the t -th hypothesis is rejected and $d_t = 0$ if it is not. Similarly, r_t denotes the truth at time t , i.e., $r_t = 1$ if $H_{0,t}$ is true, $r_t = 0$ otherwise. We also introduce the notation $\mathbf{d} = (d_1, \dots, d_T)$, $\mathbf{r} = (r_1, \dots, r_T)$. We define the true positive rate (TPR) as the ratio between the number of times where the decision correctly identifies a changepoint, and the number of positive decisions. That is

$$\text{TPR}(\mathbf{d}, \mathbf{r}) = \frac{1}{D} \sum_{t=1}^T d_t r_t,$$

where $D = \sum_{t=1}^T d_t$. We consider the compound loss function

$$L(\mathbf{d}, \mathbf{r}) = -\text{TPR}(\mathbf{d}, \mathbf{r}) + \lambda \text{ER}(\mathbf{d}, \mathbf{r}),$$

where λ is a positive constant, and, in order to penalize false detections at each time t , the error rate (ER) is defined as the ratio between the total number of false detections in the set of timepoints \mathcal{G}_t and the number of positive decisions D . That is

$$\begin{aligned} \text{ER}(\mathbf{d}, \mathbf{r}) &= \frac{1}{D} \left\{ \sum_{t=2}^T d_{t-1}(1 - r_{t-1}) + \sum_{t=1}^T d_t(1 - r_t) + \sum_{t=1}^{T-1} d_{t+1}(1 - r_{t+1}) \right\} \\ &= \frac{1}{D} \left\{ d_1(1 - r_1) + 3 \sum_{t=1}^T d_t(1 - r_t) + d_T(1 - r_T) \right\}. \end{aligned} \quad (16)$$

We aim to minimize the posterior expected loss with respect to \mathbf{d} . Then, following steps similar to those in Theorem 1 of Müller et al. (2004), it is possible to show that the optimal decision rule coincides with setting a threshold on the posterior probabilities PPC_t . Additionally, because the expression for the error rate in equation (16) includes the term $3 \sum_{t=1}^T d_t(1 - r_t)$, the resulting non-marginal Bayesian FDR, denoted as BFDR_{nm} , can be controlled such that $\text{BFDR}_{\text{nm}}(h) = 3 \text{BFDR}_{\text{m}}(h)$, where BFDR_{m} is defined in (15). Thus, it is possible to control the non-marginal BFDR_{nm} by computing the commonly used marginal Bayesian FDR and considering a more stringent level, say $\zeta/3$, for the identification of the optimal threshold on the PPC_t 's. This correction becomes especially relevant when dealing with autoregressive data, which are characterized by higher structural dependence.

4 SIMULATION STUDIES

We present two simulation studies to illustrate the performance of our LLDPM when analyzing data from different data-generating mechanisms. Specifically, we investigate the model's ability to accurately detect changepoints in both independent and autocorrelated data scenarios, while also recovering the time-specific latent cluster structure. For comparison, we evaluate our model against four alternatives:

1. The Dependent Random Partition Model (DRPM) introduced by Page et al. (2022), which, to our knowledge, is the only model-based approach that introduces time dependence directly through partitions.
2. The Linear Dependent Dirichlet Process (LDDP) by Quintana et al. (2022), which incorporates time explicitly within the atoms of the dependent process.
3. The Weighted Dependent Dirichlet Process (WDDP) by Quintana et al. (2022), which integrates time into the weights of the Dirichlet process.

n	Measure	LLDPM	DRPM	LDDP	WDDP	GMDDP
20	specificity	0.6104 (0.413)	0.6106 (0.413)	0.566 (0.288)	0.3796 (0.021)	1.000 (0.000)
	accuracy	0.9902 (0.010)	0.6288 (0.375)	0.6008 (0.265)	0.4292 (0.019)	1.000 (0.000)
	recall	1.000 (0.000)	0.8375 (0.196)	1.000 (0.000)	1.000 (0.000)	1.000 (0.000)
	precision	0.9014 (0.094)	0.4209 (0.367)	0.2714 (0.238)	0.123 (0.004)	1.000 (0.000)
	F1	0.9455 (0.054)	0.4724 (0.337)	0.3836 (0.243)	0.2191 (0.006)	1.000 (0.000)
	AUC	0.9947 (0.006)	0.7263 (0.194)	0.6472 (0.176)	0.6898 (0.010)	1.000 (0.000)
50	specificity	0.6309 (0.396)	0.6317 (0.397)	0.1961 (0.131)	0.0233 (0.021)	0.9989 (0.008)
	accuracy	0.9664 (0.023)	0.6558 (0.363)	0.2604 (0.121)	0.1014 (0.020)	0.9990 (0.007)
	recall	1.000 (0.000)	0.9325 (0.098)	1.000 (0.000)	1.000 (0.000)	1.000 (0.000)
	precision	0.7331 (0.149)	0.4292 (0.343)	0.0995 (0.013)	0.0818 (0.002)	0.9924 (0.054)
	F1	0.8378 (0.097)	0.5123 (0.330)	0.1808 (0.022)	0.1512 (0.002)	0.9952 (0.034)
	AUC	0.9817 (0.012)	0.7821 (0.193)	0.5961 (0.066)	0.5116 (0.011)	0.9995 (0.004)
100	specificity	0.6228 (0.355)	0.6146 (0.352)	0.1397 (0.126)	0.02717 (0.022)	0.9839 (0.080)
	accuracy	0.9514 (0.031)	0.6390 (0.321)	0.2086 (0.116)	0.1050 (0.020)	0.9852 (0.073)
	recall	1.0000 (0.000)	0.9200 (0.123)	1.0000 (0.000)	1.0000 (0.000)	1.0000 (0.000)
	precision	0.6611 (0.167)	0.3444 (0.281)	0.0934 (0.013)	0.0821 (0.002)	0.9671 (0.163)
	F1	0.7843 (0.118)	0.4408 (0.281)	0.1707 (0.021)	0.1517 (0.003)	0.9721 (0.138)
	AUC	0.9740 (0.017)	0.7673 (0.168)	0.5685 (0.063)	0.5134 (0.011)	0.9920 (0.040)

Table 1: Section 4.1. Performance measures for changepoint detection with independent data, for the LLDPM and four competing models. The values correspond to the average (standard errors) over 50 simulations.

4. The Griffiths–Milne Dependent Dirichlet Process (GMDDP) introduced by [Lijoi et al. \(2014\)](#) and implemented in the R package `BNPmix` ([Corradin et al., 2021](#)), which defines multivariate vectors of dependent and identically distributed Dirichlet processes.

It is important to note that, among the four alternatives we consider, the last three models are not explicitly designed to model the evolution of random partitions. To implement them for the purpose of changepoint detection, the data must be consolidated into a vector with time treated as a covariate. In contrast, the DRPM and our model are inherently model-based and do not require data concatenation to introduce time dependence. Additionally, since the alternative approaches are not specifically designed to detect changepoints in the evolution of partitions over time, they typically identify many changepoints (false detections), unless we adopt a more liberal approach when calculating the similarity between partitions at consecutive time steps. Specifically, we identify a changepoint only if the similarity between partitions at consecutive time points is less than 90% based on the ARI. This rule seemed to enhance the performance of all competitor models.

4.1 SIMULATIONS WITH INDEPENDENT DATA

We begin by simulating independent data characterized by similar partition structures over different intervals of time, trying to mimic the data-generating process characterizing the LLDPM. We

evaluate performance across 50 replicated datasets and different numbers of observations, specifically $n = \{20, 50, 100\}$, over $T = 100$ time points. In each scenario, we consider data partitions characterized by eight changepoints. At each time point, given the time-specific partition, we generate the observations for each cluster from a Normal distribution. The means of these are simulated from a Normal distribution with zero mean and variance 0.25, while the variance is common across components and set to 0.01. An example of the generated data is shown in Figure C.8 in the Supplementary Material.

To analyze these data, the specification of the LLDPM is completed as follows. We set the base partition distribution $p^*(\cdot) = p_{\text{CRP}}(\cdot)$ and the corresponding concentration parameter $\theta = 1$. The distribution $P_0(\cdot)$ is assumed Normal with mean zero and variance ζ^2 . We further specify the following hyperprior distributions: $\tau^2 \sim \text{Inv-Gamma}(15, 3)$ and $\zeta^2 \sim \text{Inv-Gamma}(15, 3)$. Additionally, we set $\eta_t \stackrel{\text{iid}}{\sim} \text{Beta}(0.1, 0.9)$, which assigns a higher probability to the absence of a changepoint at each time. When fitting the DRPM model, we set the parameters as suggested in Page et al. (2022), except for the variances, which we fixed as we did in our model. The temporal dependence parameter in the DRPM model is modeled as the analogous parameter in the LLDPM. Given the different parameterizations of the two models, this corresponds to a Beta(0.9, 0.1) distribution. Finally, for all other alternative models, we used the same variances as in our model and specified the default hyperprior parameter values.

We implemented the Gibbs sampling scheme that was detailed in Section 3. We ran the algorithm for 10,000 iterations, with the first half discarded as burn-in. Subsequently, we calculated the optimal partition for each time point based on the estimated posterior similarity matrix and the estimated posterior probability η_t , for $t = 1, \dots, T$. To determine whether a specific time point t should be considered a changepoint, we employed the Bayesian False Discovery Rate method (Newton et al., 2004; Müller et al., 2006). As explained in Section 3, we implemented a penalized version of FDR with a control level set at $(0.01/3)$.

Table 1 presents the performance of the five models across varying data dimensions. Remarkably, the LLDPM consistently outperforms all other models across all metrics. However, as the sample size increases, all models show a decrease in performance due to the higher likelihood of subjects switching clusters. The results underscore the robust performance of GMDDP in metrics related to changepoint detection. At the same time, when evaluating the accuracy of recovering the true latent cluster structure, depicted in Figure 3, GMDDP struggles and does not accurately identify clusters. Therefore, GMDDP may not be optimal when simultaneous changepoint detection and cluster analysis are required. Also the DRPM shows robust performance in changepoint detection, with an average specificity comparable to our model in each scenario. However, its ability to recover the correct cluster structure diminishes as the number of subjects increases. In contrast, LLDPM demonstrates excellent performance in both changepoint detection and recovering the latent cluster structure.

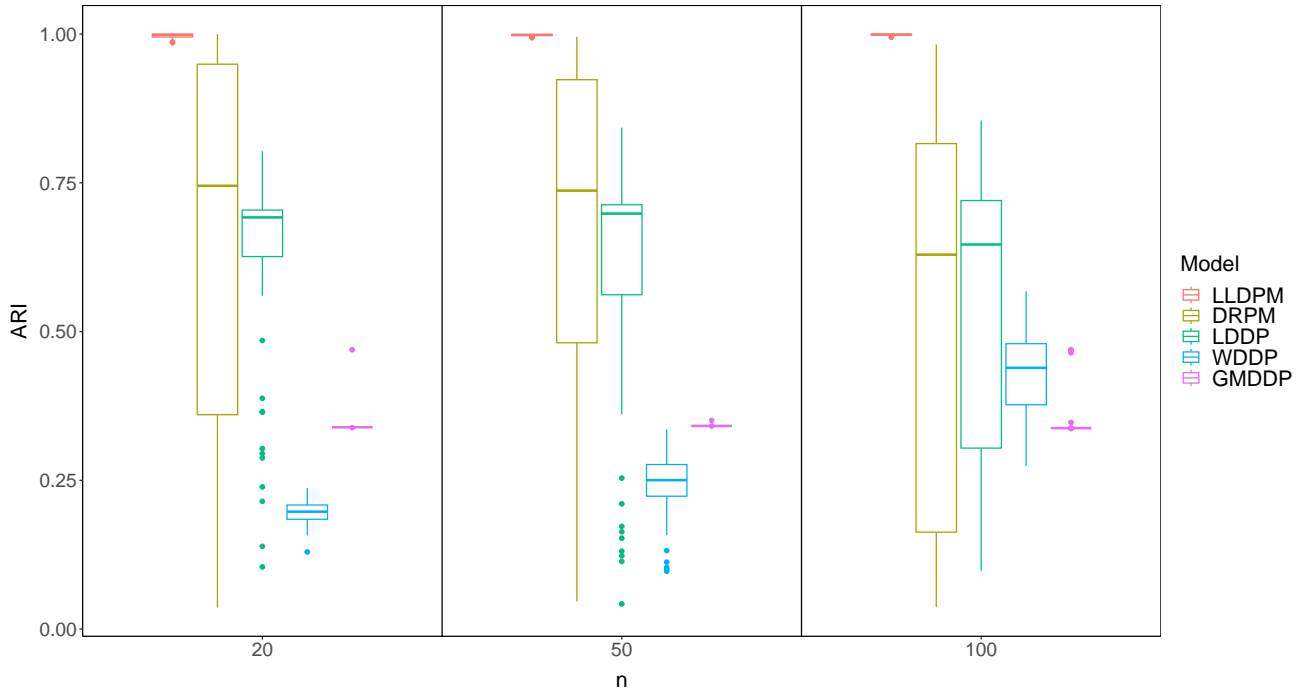


Figure 3: Section 4.1. Boxplots of the average ARI, to evaluate the clustering performance when analyzing independent data, for our model and four alternatives, with $n = \{20, 50, 100\}$. Results are based on 50 replicated datasets and averaged over 100 time points. For each dataset and each method, at each time point, the true partition is compared with the partition estimated by minimizing the lower bound of the posterior expected Variation of Information.

4.2 SIMULATIONS WITH AUTOREGRESSIVE DATA

In a second simulation study, we aim to assess the performance of our LLDPM in scenarios where the data are generated from a process characterized by an autoregressive structure of order one, or AR(1). Specifically, we consider datasets with $T = 30$ time points and $n = 20$ units, generated from the model

$$Y_{i,t} = \lambda Y_{i,t-1} + \tilde{\beta}_{i,t} + \tilde{\varepsilon}_i,$$

where the error terms $\tilde{\varepsilon}_i$ are assumed to be independent and identically distributed from a Normal with mean zero and variance one. At each time point $t = 1, \dots, T$, units are partitioned based on the distinct values taken by $\tilde{\beta}_{i,t}$. The number of distinct values of $\tilde{\beta}_{i,t}$, and hence the number of clusters, ranges between one and three. Specifically, it is equal to three if t is divisible by five, it is equal to two if t is divisible by nine, and it is equal to one otherwise. The individual allocation of the units to clusters changes every time the number of clusters changes. An example of such data is shown in Figure C.9 in the Supplementary Material. When fitting our model we set θ according to the resulting expected prior number of cluster, which for the LLDPM with specification $p^*(\cdot) = p_{\text{CRP}}(\cdot)$ is given by $\mathbb{E}[|\pi_t|] = \sum_{i=1}^n \theta / (\theta + i - 1)$ (Pitman, 2002), for every $t = 1, \dots, T$. We thus set $\theta = 0.32$, corresponding

λ	Measure	LLDPM	DRPM	LDDP	WDDP	GMDDP
0.25	specificity	0.8683 (0.151)	0.8728 (0.152)	0.9971 (0.014)	0.8121 (0.066)	0.7700 (0.125)
	accuracy	0.9147 (0.059)	0.5156 (0.044)	0.9987 (0.006)	0.5029 (0.032)	0.6173 (0.068)
	recall	0.9175 (0.073)	0.2031 (0.097)	1.000 (0.000)	0.2323 (0.063)	0.4838 (0.065)
	precision	0.9252 (0.065)	0.7473 (0.211)	0.9976 (0.012)	0.6043 (0.132)	0.7219 (0.115)
	F1	0.9195 (0.055)	0.2972 (0.095)	0.9988 (0.006)	0.3280 (0.078)	0.5743 (0.064)
	AUC	0.9145 (0.059)	0.5284 (0.040)	0.9986 (0.007)	0.5204 (0.031)	0.6308 (0.063)
0.5	specificity	0.9082 (0.177)	0.9059 (0.178)	0.9943 (0.020)	0.8111 (0.061)	0.5514 (0.198)
	accuracy	0.8913 (0.066)	0.5276 (0.039)	0.9973 (0.009)	0.5015 (0.036)	0.5800 (0.100)
	recall	0.9038 (0.082)	0.1966 (0.134)	1.000 (0.000)	0.2306 (0.070)	0.6050 (0.104)
	precision	0.8992 (0.074)	0.8368 (0.208)	0.9953 (0.016)	0.5772 (0.085)	0.6219 (0.111)
	F1	0.8984 (0.061)	0.2886 (0.109)	0.9976 (0.008)	0.3249 (0.088)	0.6059 (0.082)
	AUC	0.8904 (0.066)	0.5421 (0.044)	0.9971 (0.010)	0.5188 (0.034)	0.5866 (0.097)
0.75	specificity	0.9226 (0.081)	0.9286 (0.066)	0.9671 (0.065)	0.7726 (0.071)	0.3514 (0.299)
	accuracy	0.8707 (0.060)	0.5352 (0.036)	0.9847 (0.030)	0.4993 (0.061)	0.6533 (0.156)
	recall	0.8838 (0.082)	0.1910 (0.077)	1.000 (0.000)	0.2602 (0.122)	0.9175 (0.092)
	precision	0.8862 (0.089)	0.7940 (0.168)	0.9747 (0.049)	0.5618 (0.089)	0.6383 (0.139)
	F1	0.8797 (0.062)	0.2972 (0.096)	0.9866 (0.026)	0.3474 (0.102)	0.7458 (0.107)
	AUC	0.8697 (0.062)	0.5430 (0.040)	0.9836 (0.032)	0.5161 (0.058)	0.6345 (0.164)
0.9	specificity	0.9127 (0.095)	0.9143 (0.096)	0.4586 (0.296)	0.7500 (0.094)	0.2811 (0.269)
	accuracy	0.8533 (0.056)	0.5181 (0.054)	0.7407 (0.141)	0.4680 (0.052)	0.6290 (0.133)
	recall	0.8600 (0.078)	0.1714 (0.091)	0.9875 (0.028)	0.2213 (0.066)	0.9334 (0.157)
	precision	0.8701 (0.072)	0.7380 (0.223)	0.6977 (0.130)	0.5090 (0.131)	0.6020 (0.149)
	F1	0.8618 (0.053)	0.2648 (0.123)	0.8112 (0.089)	0.3041 (0.081)	0.7420 (0.083)
	AUC	0.8529 (0.057)	0.5300 (0.050)	0.7230 (0.150)	0.4856 (0.053)	0.5987 (0.136)

Table 2: Section 4.2. Performance measures for changepoint detection with AR(1) data, for the LLDPM and four competing models. The values correspond to the average (standard errors) over 50 simulations.

to $\mathbb{E}[|\pi_t|] = 2$. For the other parameters, we use the same specifications as in the first simulation study (see Section 4.1). As before, we run the MCMC for 10,000 iterations, discarding the first half.

The results of our analysis, based on 50 replicates, are presented in Table 2. The LLDPM consistently excels in identifying changepoints across all metrics considered. In this second scenario, the GMDDP shows reduced effectiveness compared to the previous simulation study. The LDDP demonstrates strong ability in identifying changepoints; however, similar to the GMDDP in the previous study, it is less reliable in accurately identifying the cluster structure. Figure 4 illustrates that our LLDPM outperforms the other methods in recovering the correct latent cluster allocations, with ARI indices consistently above 0.7 for data generated with different autoregressive coefficients.

Considering both scenarios together, our approach appears to provide reliable inference both for changepoint detection and cluster allocation with respect to the competing approaches considered here.

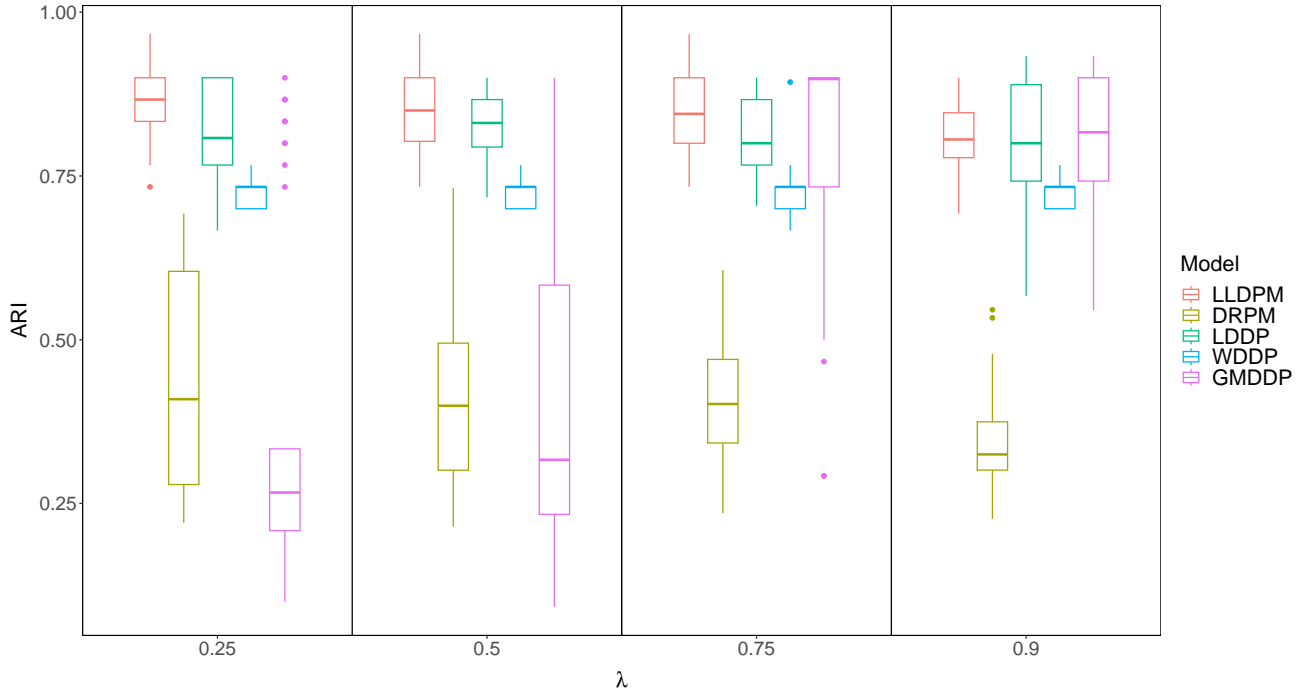


Figure 4: Section 4.2. Boxplots of the average ARI to evaluate the clustering performance when analyzing AR(1) data, for our model and four alternatives, and different values of the autoregressive coefficient $\lambda = \{0.25, 0.5, 0.75, 0.9\}$. Results are based on 50 replicated datasets and averaged over 30 time points. For each dataset and each method, at each time point, the true partition is compared with the partition estimated by minimizing the lower bound of the posterior expected Variation of Information.

5 APPLICATION TO GESTURE PHASE SEGMENTATION

We present an analysis of video-recorded data for human gesture segmentation. The goal is to segment videos into distinct phases exhibiting different motion patterns, e.g., to identify time lapses of the video that need to be removed from a clip (Parvathy et al., 2021). More specifically, we employ the Gesture Phase Segmentation dataset, originally described by Madeo et al. (2013), which is publicly accessible for download at the following URL: <https://archive.ics.uci.edu/ml/datasets/gesture+phase+segmentation>. While Madeo et al. (2013) analyzed this dataset using Support Vector Machines (SVM) to segment, and classify gesture data streams, they did not consider partitioning gesture phases into their components and investigating the temporal dependence between partitions. Our goal, in contrast, is to detect the latent cluster structure at each frame while capturing changepoints, using our proposed LLDPM random partition model with time dependence.

The dataset contains sensor data recordings of users recounting comic book stories facing an Xbox Microsoft KinectTM sensor. The dataset provides scalar velocity and acceleration values over four sensors, placed on the left hand, right hand, left wrist, and right wrist, leading to $n = 8$ sensor measurements at regular time intervals (frames). These values were obtained by normalizing hand and

wrist positions relative to the head and spine position using a fixed displacement offset of 3 to measure velocity. Our analysis is based on a processed version of the data, which we prepare following the approach outlined by [Hadj-Amar et al. \(2024\)](#). The preprocessing involves four stages:

- i) Smoothing. We apply a two-point moving average filter to smooth the time series.
- ii) Downsampling. To reduce the data volume while preserving essential patterns, we select every fifth data point, as suggested by [Romanuke \(2021\)](#). This technique allows us to handle longer time lags while minimizing parameters and computational complexity.
- iii) Transformation. We apply a square root transformation, which [Hadj-Amar et al. \(2024\)](#) found to be effective in fitting a Gaussian distribution to the data.
- iv) Standardization. We standardize the time series to ensure uniformity and comparability across the dataset.

The processed data is illustrated in Figure 5. For additional context, see Figure D.10 in the Supplementary Material, which plots the data along with details on the video phases previously identified by [Madeo et al. \(2013\)](#): D (rest position, from the Portuguese “descanso”), P (preparation), S (stroke), H (hold), and R (retraction).

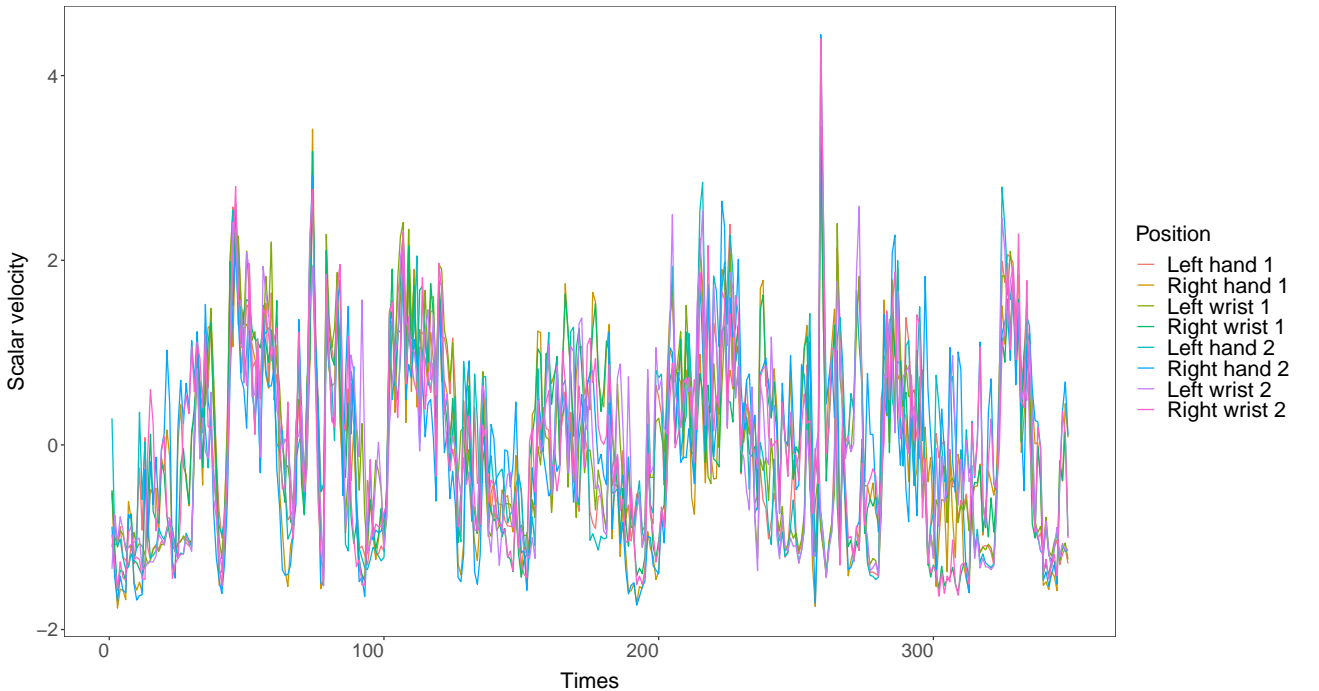


Figure 5: Section 5, Human Gesture data. Scalar velocity of the left and right hand and the wrists after preprocessing ($T = 349$).

Here, we illustrate our model’s performance in analyzing this data. Gesture phase segmentation poses several challenges. Firstly, it is inherently subjective, with no definitive starting point for each

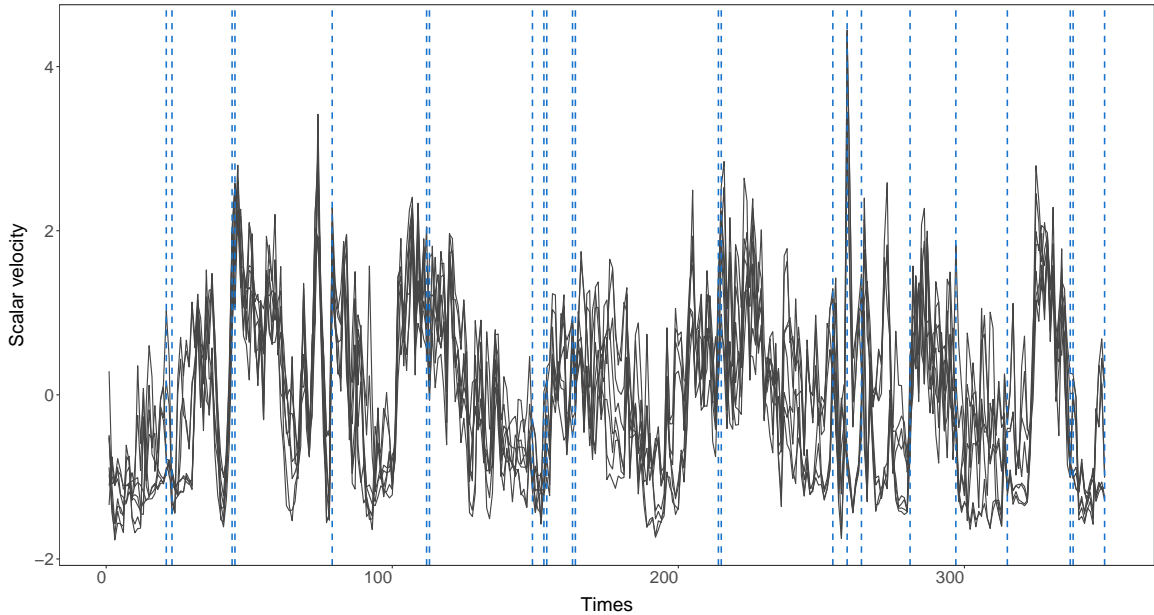


Figure 6: Section 5, Human Gesture data. Changepoints (dashed line) identified with the LLDPM.

phase, leading to varying segmentations by different experts for the same video. Additionally, similar patterns may occur across different activities; for example, stationary hand gestures may be seen in both the rest and hold phases identified by [Madedo et al. \(2013\)](#). Furthermore, the data may include nuisance movements, such as touching glasses while speaking, which can cause fluctuations in sensor-recorded scalar velocity ([Madedo et al., 2013](#)). To implement the LLDPM, we consider an a priori expected number of clusters equal to two at each time point, corresponding to the specification $\theta = 0.5$ for the concentration parameter of the CRP. The prior probability of a changepoint is assumed $\eta_t \stackrel{\text{iid}}{\sim} \text{Beta}(0.1, 0.9)$, suggesting that the model assumes a relatively low prior probability of a changepoint at each time point. For the distribution $P_0(\cdot)$ of the coefficients $\beta_{i,t}$, we assume a Normal distribution with a mean zero and variance $\zeta^2 = 0.5^2$. Finally, $\tau^2 \sim \text{Inv-Gamma}(15, 3)$. We run our MCMC algorithm for 10,000 iterations, with the first half discarded as a burn-in.

The estimated changepoints are displayed in Figure 6 and appear distributed throughout the time series, possibly indicating that the person wearing the sensors is gesticulating while recalling the comic story. When compared with the segmentation in [Madedo et al. \(2013\)](#), the changepoints identified by the LLDPM primarily occur during the activity phase, which correspond to the preparation, retraction, and stroke phases in the video. Additionally, most of these changepoints are observed during transitions between different phases, with a notable increase in frequency during the reading phases. These changepoints likely reflect movements related to the subject’s gesticulation and body language while narrating, as well as shifts in hand and wrist positions during the assigned activity. Figure 7 illustrates the clustering of the eight sensors within a specific time window, chosen for representation purposes. The estimated clustering is obtained by minimizing the lower bound of the posterior expected Variation

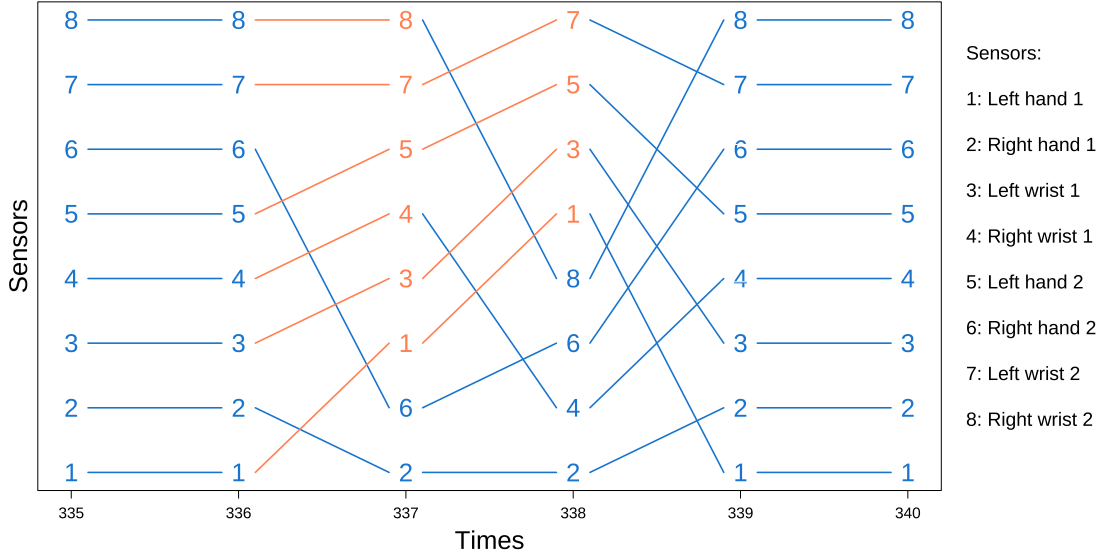


Figure 7: Section 5, Human Gesture Data. Time-specific clusters obtained by minimizing the lower bound of the posterior expected Variation of Information, for the time window from time 335 to time 340. Numbers refer to the measurements of scalar velocity (1-4) and acceleration (5-8) in sensor units placed on the hands and wrists of a subject, whereas colors indicate clusters.

of Information. The numbers on the plot correspond to the sensor measurements. Notably, a distinct pattern allocation emerges, where all the sensors are grouped into a single primary cluster. Additionally, a secondary pattern takes shape, forming two clusters: one containing all the sensors from the left arm (odd numbers) and the other with sensors from the right arm (even numbers) grouped together.

For comparison, we analyzed the same data with the alternative models considered in this work. The identified changepoints are displayed in Figures, D.11, D.12, D.13 and D.14 in the Supplementary Material. It is notable that partition-based models appear to identify fewer changepoints. For instance, the DRPM detected only 15 changepoints (4.3% of the total time points), primarily at the beginning of the time series, and the LLDPM identified 23 changepoints (6.6%). In contrast, the other alternative models, namely the LDDP, WDDP, and GMDDP, identified approximately 14% of the changepoints, with 48, 50, and 51 changepoints, respectively, out of 349 time points. These observations instill confidence in the performance of the LLDPM, which thus might be a reliable modeling option, particularly in real-world applications where the ground truth is unknown.

6 DISCUSSION

We introduced a new approach for modeling partitions with temporal dependence that relies on the definition of partition-based state equations in a state-space model, thus extending the Dynamic Linear Model widely used in multivariate time series analysis. By characterizing the evolution of the local

level equation across partitions and detecting changepoints, our model effectively captures changes in cluster structures over time. Our approach maximizes the use of temporal information while introducing dependence only when supported by the data. This is achieved by incorporating a spike-and-slab formulation to model independence between partitions, thereby enhancing model flexibility. We have illustrated the model’s performance using synthetic data, which highlighted its accuracy in recovering cluster structures and correctly identifying changepoints. In an application to human gesture data, our model provides reasonable results, particularly in identifying most of the changepoints during activity phases. These results offer valuable insights into the mechanics of human movement and have the potential to significantly enhance gesture recognition systems. Furthermore, the partitions estimated by our random partition model could be integrated as predictors into broader outcome models. For instance, they could be used to determine how different gesture intervals are associated with a propensity for risk-taking or other behavioral outcomes. Thus, understanding these gesture phase clusters can lead to a deeper insight into human behavior, accounting for all probabilistic uncertainties.

Drawing upon the framework presented in Section 2.2, our model can be extended to analyze multivariate data across multiple sources, where dependences arise beyond temporal factors, e.g., varying experimental conditions. This adaptation allows our model to accommodate diverse data structures and complex inter-condition dependences. Importantly, even in this extended context, the random partitions maintain a marginal identical distribution, e.g. the distribution of a Chinese restaurant process. This underscores the model’s adaptability and versatility in capturing complex dependences across different datasets.

Finally, an exciting avenue for future research is the development of dependent random partition state-space models capable of modeling latent state equations that encode more complex dynamics. This extension could encompass higher-order time dependences, allowing for exploring more complex temporal relationships and patterns in data. In order to ensure smoother transitions over time, a hierarchical model formulation could shrink the base partition distribution $p^*(\pi)$ to the partition estimated at time $t - 1$ or a fixed “anchor” partition. However, care will be needed to ensure computational feasibility and interpretability of the parameters γ . See, e.g., Paganin et al. (2021) or Dahl et al. (2023) for details on recently proposed anchored partitioned models. Similarly, we have assumed that the change point selection indicator $\gamma_{i,t}$ is independent across times. More in general, the changepoint selection could depend on time-varying covariates, such as respiratory data or measurements of expended effort in the analysis of human gesture data. Such developments have the potential to significantly enhance our ability to capture and understand time-varying clustering structures in complex time series data across a wide range of domains and applications.

REFERENCES

- Antoniano-Villalobos, I. and S. G. Walker (2016). A nonparametric model for stationary time series. *Journal of Time Series Analysis* 37(1), 126–142. [3](#)
- Arbel, J., S. Favaro, B. Nipoti, and Y. W. Teh (2017). Bayesian nonparametric inference for discovery probabilities: Credible intervals and large sample asymptotics. *Statistica Sinica*, 839–858. [7](#)
- Barry, D. and J. A. Hartigan (1992). Product partition models for change point problems. *The Annals of Statistics*, 260–279. [3](#)
- Beraha, M., A. Guglielmi, F. A. Quintana, M. de Iorio, J. G. Eriksson, and F. Yap (2022). Bayesian nonparametric vector autoregressive models via a logit stick-breaking prior: an application to child obesity. *arXiv preprint arXiv:2203.12280*. [3](#)
- Blackwell, D., J. B. MacQueen, et al. (1973). Ferguson distributions via pólya urn schemes. *The Annals of Statistics* 1(2), 353–355. [3](#)
- Caron, F., M. Davy, and A. Doucet (2007). Generalized Pólya urn for time-varying Dirichlet process mixtures. In *Proceedings of the Twenty-Third Conference on Uncertainty in Artificial Intelligence, UAI'07*, Arlington, Virginia, USA, pp. 33–40. AUAI Press. [3](#)
- Caron, F., W. Neiswanger, F. Wood, A. Doucet, and M. Davy (2017). Generalized pólya urn for time-varying pitman-yor processes. *Journal of Machine Learning Research* 18(27). [3](#)
- Cassese, A., W. Zhu, M. Guindani, and M. Vannucci (2019). A Bayesian Nonparametric Spiked Process Prior for Dynamic Model Selection. *Bayesian Analysis* 14(2), 553 – 572. [3](#)
- Chandra, N. K. and S. Bhattacharya (2019). Non-marginal decisions: A novel bayesian multiple testing procedure. *Electronic Journal of Statistics* 13(1), 1535–1570. [5](#), [15](#)
- Corradin, R., A. Canale, and B. Nipoti (2021). Bnpmix: An r package for bayesian nonparametric modeling via pitman-yor mixtures. *Journal of Statistical Software* 100, 1–33. [17](#)
- Dahl, D. B., R. L. Warr, and T. P. Jensen (2023). Dependent random partitions by shrinking toward an anchor. *arXiv preprint arXiv:2312.17716*. [25](#)
- De Blasi, P., S. Favaro, A. Lijoi, R. H. Mena, I. Prünster, and M. Ruggiero (2013). Are gibbs-type priors the most natural generalization of the Dirichlet process? *IEEE transactions on pattern analysis and machine intelligence* 37(2), 212–229. [7](#)
- De Iorio, M., S. Favaro, A. Guglielmi, and L. Ye (2019). Bayesian nonparametric temporal dynamic clustering via autoregressive Dirichlet priors. *arXiv preprint arXiv:1910.10443*. [3](#)

- DeYoreo, M. and A. Kottas (2018). Modeling for dynamic ordinal regression relationships: An application to estimating maturity of rockfish in california. *Journal of the American Statistical Association* 113(521), 68–80. [3](#)
- Dombowsky, A. and D. B. Dunson (2023). Product centered dirichlet processes for dependent clustering. *arXiv preprint arXiv:2312.05365*. [5](#), [9](#), [11](#)
- Ferguson, T. S. (1973). A bayesian analysis of some nonparametric problems. *The Annals of Statistics*, 209–230. [3](#), [7](#)
- Franzolini, B., M. De Iorio, and J. Eriksson (2023). Conditional partial exchangeability: a probabilistic framework for multi-view clustering. *arXiv preprint arXiv:2307.01152*. [5](#), [11](#)
- Gnedin, A. V. and J. Pitman (2005). Exchangeable gibbs partitions and stirling triangles. *Записки научных семинаров ПОМИ* 325(0), 83–102. [7](#)
- Hadj-Amar, B., J. Jewson, and M. Vannucci (2024). Bayesian sparse vector autoregressive switching models with application to human gesture phase segmentation. *Annals of Applied Statistics to appear*. [22](#)
- Hartigan, J. A. (1990). Partition models. *Communications in statistics-Theory and methods* 19(8), 2745–2756. [3](#)
- Kalli, M. and J. E. Griffin (2018). Bayesian nonparametric vector autoregressive models. *Journal of Econometrics* 203(2), 267–282. [3](#)
- Lijoi, A., R. H. Mena, and I. Prünster (2005). Hierarchical mixture modeling with normalized inverse-gaussian priors. *Journal of the American Statistical Association* 100(472), 1278–1291. [7](#)
- Lijoi, A., R. H. Mena, and I. Prünster (2007). Controlling the reinforcement in bayesian non-parametric mixture models. *Journal of the Royal Statistical Society Series B: Statistical Methodology* 69(4), 715–740. [7](#)
- Lijoi, A., B. Nipoti, and I. Prünster (2014). Bayesian inference with dependent normalized completely random measures. *Bernoulli*. [17](#)
- Madeo, R. C., C. A. Lima, and S. M. Peres (2013). Gesture unit segmentation using support vector machines: segmenting gestures from rest positions. In *Proceedings of the 28th Annual ACM Symposium on Applied Computing*, pp. 46–52. [21](#), [22](#), [23](#), [36](#)
- Martinez, A. F. and R. H. Mena (2014). On a nonparametric change point detection model in markovian regimes. *Bayesian Analysis*. [3](#)

- Müller, P., G. Parmigiani, and K. Rice (2006). Fdr and bayesian multiple comparisons rules. *Proc. Valencia / ISBA 8th World Meeting on Bayesian Statistics*. [15](#), [18](#)
- Müller, P., G. Parmigiani, C. Robert, and J. Rousseau (2004). Optimal sample size for multiple testing: the case of gene expression microarrays. *Journal of the American Statistical Association* *99*(468), 990–1001. [15](#), [16](#)
- Neal, R. M. (2000). Markov chain sampling methods for Dirichlet process mixture models. *Journal of Computational and Graphical Statistics* *9*(2), 249–265. [12](#)
- Newton, M. A., A. Noueir, D. Sarkar, and P. Ahlquist (2004). Detecting differential gene expression with a semiparametric hierarchical mixture method. *Biostatistics* *4*(1), 155–176. [15](#), [18](#)
- Nieto-Barajas, L. E. and A. Contreras-Cristán (2014). A bayesian nonparametric approach for time series clustering. *Bayesian Analysis* *9*(1), 147–170. [3](#)
- Paganin, S., A. H. Herring, A. F. Olshan, D. B. Dunson, and N. B. D. P. Study (2021, Mar). Centered partition processes: Informative priors for clustering (with discussion). *Bayesian Analysis* *16*(1), 301–370. [25](#)
- Page, G. L., F. A. Quintana, and D. B. Dahl (2022). Dependent modeling of temporal sequences of random partitions. *Journal of Computational and Graphical Statistics* *31*(2), 614–627. [3](#), [4](#), [8](#), [16](#), [18](#), [30](#)
- Parvathy, P., K. Subramaniam, G. Prasanna Venkatesan, P. Karthikaikumar, J. Varghese, and T. Jayasankar (2021). Development of hand gesture recognition system using machine learning. *Journal of Ambient Intelligence and Humanized Computing* *12*, 6793–6800. [21](#)
- Petris, G., S. Petrone, and P. Campagnoli (2009). *Dynamic linear models with R*. Springer Science & Business Media. [2](#)
- Pitman, J. (2002). Combinatorial stochastic processes lecture notes for st. flour summer school. [7](#), [19](#)
- Pitman, J. and M. Yor (1997). The two-parameter poisson-Dirichlet distribution derived from a stable subordinator. *The Annals of Probability*, 855–900. [7](#)
- Quinlan, J. J., G. L. Page, and L. M. Castro (2022). Joint random partition models for multivariate change point analysis. *Bayesian Analysis* *1*(1), 1–28. [3](#)
- Quintana, F. A., P. Müller, A. Jara, and S. N. MacEachern (2022). The dependent Dirichlet process and related models. *Statistical Science* *37*(1), 24–41. [2](#), [16](#)

- Rand, W. M. (1971). Objective criteria for the evaluation of clustering methods. *Journal of the American Statistical Association* 66(336), 846–850. [8](#)
- Romanuke, V. (2021). Time series smoothing improving forecasting. *Applied Computer Systems* 26(1), 60–70. [22](#)
- Sethuraman, J. (1994). A constructive definition of Dirichlet priors. *Statistica sinica*, 639–650. [3](#)
- Sun, W. and T. T. Cai (2007). Oracle and adaptive compound decision rules for false discovery rate control. *Journal of the American Statistical Association* 102, 901–912. [14](#)
- Sun, W., B. J. Reich, T. T. Cai, M. Guindani, and A. Schwartzman (2015). False discovery control in large-scale spatial multiple testing. *Journal of the Royal Statistical Society, Series B: Statistical Methodology* 77, 59–80. [15](#)
- Tadesse, M. G. and M. Vannucci (2021). Handbook of bayesian variable selection. *Chapman & Hall/CRC*. [5](#)

SUPPLEMENTARY MATERIAL

The Supplementary Material is organized as follows. In Section A we provide the proofs of the results in Section 2 of the main article. Section B provides additional details on posterior computations. Finally, Sections C and D report further information on the simulation studies and the application, in Sections 4 and 5 of the main article.

A PROOFS

A.1 PROOF OF PROPOSITION 1

Proof. We let $c_{i,t}$, for $i = 1, \dots, n$ and $t = 1, \dots, T$, be a random variable taking values in $\{1, \dots, |\pi_t|\}$, such that $c_{i,t} = j$ if $i \in C_{j,t}$. As observed in Page et al. (2022), the ERI can be written as

$$\varphi_{t_1, t_2} = \mathbb{E}[R(\pi_{t_1}, \pi_{t_2})] = \binom{n}{2}^{-1} \sum_{1 \leq i < j \leq n} \psi_{i,j},$$

where $\psi_{i,j} = P(c_{i,t_1} = c_{j,t_1}, c_{i,t_2} = c_{j,t_2}) + P(c_{i,t_1} \neq c_{j,t_1}, c_{i,t_2} \neq c_{j,t_2})$. Following exchangeability, it is easy to verify that $\varphi_{t_1, t_2} = \psi_{1,2}$. From the predictive distribution of a Gibbs-type prior, we obtain $P(c_{1,t_1} = c_{2,t_1}) = V_{2,1}(1 - \sigma)$ and $P(c_{1,t_1} \neq c_{2,t_1}) = V_{2,2}$. Moreover,

$$P(c_{1,t_2} = c_{2,t_2} \mid c_{1,t_1} = c_{2,t_1}, \gamma_{t_2}) = \begin{cases} 1 & \text{if } \gamma_{t_2} = 0 \\ V_{2,1}(1 - \sigma) & \text{if } \gamma_{t_2} = 1, \end{cases}$$

and

$$P(c_{1,t_2} \neq c_{2,t_2} \mid c_{1,t_1} \neq c_{2,t_1}, \gamma_{t_2}) = \begin{cases} 1 & \text{if } \gamma_{t_2} = 0 \\ V_{2,2} & \text{if } \gamma_{t_2} = 1. \end{cases}$$

Then, we can calculate

$$\begin{aligned} P(c_{1,t_1} = c_{2,t_1}, c_{1,t_2} = c_{2,t_2}) &= P(c_{1,t_1} = c_{2,t_1}) \\ &\times \sum_{\gamma \in \{0,1\}} P(c_{1,t_2} = c_{2,t_2} \mid c_{1,t_1} = c_{2,t_1}, \gamma_{t_2} = \gamma) P(\gamma_{t_2} = \gamma) \quad (17) \\ &= V_{2,1}(1 - \sigma)(1 - \eta) + [V_{2,1}(1 - \sigma)]^2 \eta. \end{aligned}$$

Similarly,

$$\begin{aligned}
P(c_{1,t_1} \neq c_{2,t_1}, c_{1,t_2} \neq c_{2,t_2}) &= P(c_{1,t_1} \neq c_{2,t_1}) \\
&\times \sum_{\gamma \in \{0,1\}} P(c_{1,t_2} \neq c_{2,t_2} \mid c_{1,t_1} \neq c_{2,t_1}, \gamma_{t_2} = \gamma) P(\gamma_{t_2} = \gamma) \quad (18) \\
&= V_{2,2}(1 - \eta) + V_{2,2}^2 \eta.
\end{aligned}$$

The result follows by summing (17) and (18) and by recalling that $V_{1,1} = V_{2,1}(1 - \sigma) + V_{2,2}$. \square

A.2 PROOF OF PROPOSITION 2

Proof. By assumption, $\pi_1 \sim p^*(\pi_1)$. For any $t = 2, \dots, T$, we denote by $p(\pi_t)$ the distribution of π_t , which can be obtained by marginalizing the distribution of $\boldsymbol{\pi}_{1:T}$ with respect to all the remaining $T - 1$ components. We start by marginalizing it with respect to π_1 , which gives:

$$\begin{aligned}
p(\pi_t) &= \sum_{\substack{r=1 \\ r \neq t}}^T \sum_{\pi_r \in \mathcal{P}} p^*(\pi_1) \prod_{s=2}^T [(1 - \eta_s) \delta_{\pi_{s-1}}(\pi_s) + \eta_s p^*(\pi_s)] \\
&= \sum_{\substack{r=2 \\ r \neq t}}^T \sum_{\pi_r \in \mathcal{P}} \prod_{s=3}^T [(1 - \eta_s) \delta_{\pi_{s-1}}(\pi_s) + \eta_s p^*(\pi_s)] \\
&\times \sum_{\pi_1 \in \mathcal{P}} p^*(\pi_1) [(1 - \eta_2) \delta_{\pi_2}(\pi_1) + \eta_2 p^*(\pi_2)] \\
&= \sum_{\substack{r=2 \\ r \neq t}}^T \sum_{\pi_r \in \mathcal{P}} \prod_{s=3}^T [(1 - \eta_s) \delta_{\pi_{s-1}}(\pi_s) + \eta_s p^*(\pi_s)] [(1 - \eta_2) p^*(\pi_2) + \eta_2 p^*(\pi_2)] \\
&= \sum_{\substack{r=2 \\ r \neq t}}^T \sum_{\pi_r \in \mathcal{P}} p^*(\pi_2) \prod_{s=3}^T [(1 - \eta_s) \delta_{\pi_{s-1}}(\pi_s) + \eta_s p^*(\pi_s)].
\end{aligned}$$

By iterating the same procedure for the next $t - 2$ terms of the first sum, we get

$$\begin{aligned}
p(\pi_t) &= p^*(\pi_t) \sum_{r=t+1}^T \sum_{\pi_r \in \mathcal{P}} \prod_{s=t+1}^T [(1 - \eta_s) \delta_{\pi_{s-1}}(\pi_s) + \eta_s p^*(\pi_s)] \\
&= p^*(\pi_t),
\end{aligned}$$

where the last identity holds as $\prod_{s=t+1}^T [(1 - \eta_s) \delta_{\pi_{s-1}}(\pi_s) + \eta_s p^*(\pi_s)]$ is the conditional distribution of $\boldsymbol{\pi}_{(t+1):T}$ given π_t , which thus sums up to one. Then, π_t is marginally distributed as $p^*(\pi_t)$ for every $t = 1, \dots, T$. \square

B FURTHER DETAILS ON POSTERIOR COMPUTATIONS

B.1 ESTIMATING THE MARGINAL LIKELIHOOD g_t

For any $t = 1, \dots, T$, the marginal likelihood g_t , as defined in (14), can be estimated via Monte Carlo.

We observe that

$$g_t = \sum_{\pi_t \in \mathcal{P}} p_{\text{CRP}}(\pi_t) p(\mathbf{Y}_t | \pi_t) = \mathbb{E} [p(\mathbf{Y}_t | \pi)],$$

where the expected value is taken with respect to a random partition $\pi \sim p_{\text{CRP}}(\pi)$. This step is made efficient based on three considerations.

- i) Each g_t is estimated only once, before running the Gibbs sampling described in Section 3.
- ii) The same sample of partitions generated from $p_{\text{CRP}}(\cdot)$ can be used to estimate g_t for all $t = 1, \dots, T$.
- iii) If the kernel $p(y_{i,t} | \beta_{i,t})$ in (2), and the base measure $P_0(\cdot)$ are specified in a convenient form, the function $p(\mathbf{Y}_t | \pi_t)$ is available in closed-form and easy to evaluate. For example, when both are assumed normal (specifically $y_{i,t} | \beta_{i,t} \sim \text{N}(\beta_{i,t}, \tau^2)$ and $P_0(\cdot)$ Normal with mean μ and variance ς^2), as implemented in Sections 4 and 5, then

$$\begin{aligned} \log p(\mathbf{Y}_t | \pi_t) &= \sum_{j=1}^{|\pi_t|} -\frac{n_j}{2} \log(2\pi) - n_j \log \tau - \log \varsigma + \frac{1}{2} \log \frac{\tau^2 \varsigma^2}{n_j \varsigma^2 + \tau^2} \\ &\quad - \frac{1}{2} \sum_{i=1}^{n_j} y_{i,t}^2 - \frac{\mu^2}{2\varsigma^2} + \frac{\tau^2 \varsigma^2}{2(n_j \varsigma^2 + \tau^2)} \left(\frac{\mu}{\varsigma^2} + \frac{\sum_{i=1}^{n_j} y_{i,t}}{\tau^2} \right). \end{aligned}$$

B.2 RESHUFFLING STEP

Updating the partitions $\pi_{1:T}$, conditionally on $\gamma_{2:T}$, at each iteration of the Gibbs sampler helps improving the mixing of the algorithm. We discuss how this can be done efficiently. We start by observing that the values taken by $\gamma_{2:T}$ determine a partition of the partitions $\pi_{1:T}$ into $k_T \leq T$ blocks. Within each block, all partitions are identical. We introduce the notation $\{\pi_1^*, \dots, \pi_{k_T}^*\}$ to indicate the k_T partitions corresponding to the k_T blocks and we observe that there can be ties among the elements of $\{\pi_1^*, \dots, \pi_{k_T}^*\}$. For example, if $\gamma_2 = \gamma_3 = 0$ while $\gamma_4 = 1$, then the first block of partitions consists of $\pi_1^* = \pi_1 = \pi_2 = \pi_3$. The reshuffling step thus consists in updating the values π_j^* , for $j = 1, \dots, k_T$, from the corresponding full conditional distributions. If \mathcal{D}_j denotes the set of partitions assigned to the j th cluster, then the full conditional of π_j^* takes the form

$$p(\pi_j^* | \dots) \propto p_{\text{CRP}}(\pi_j^*) \prod_{l \in \mathcal{D}_j} p(\mathbf{Y}_l | \pi_j^*). \quad (19)$$

If $|\mathcal{D}_j| = 1$, say $\mathcal{D}_j = \{\pi_{t_j}\}$, for some t_j , then the problem of sampling from (19) can be tackled simply by picking an element at random from the list \mathcal{S}_{t_j} . If $|\mathcal{D}_j| > 1$, say $\mathcal{D}_j = \{\pi_{t_{j,1}}, \dots, \pi_{t_{j,|\mathcal{D}_j|}}\}$, then we propose a sampling importance resampling step to simulate from (19). Specifically,

- i. For every $r = 1, \dots, |\mathcal{D}_j|$, we sample at random $m_{t_{j,r}}$ draws from $\mathcal{S}_{t_{j,r}}$ (i.e. from the conditional distribution of $\pi_{t_{j,r}}$ given $\mathbf{Y}_{t_{j,r}}$). In total we thus get $m_j = m_{t_{j,1}} + \dots + m_{t_{j,|\mathcal{D}_j|}}$ candidate partitions from $\mathcal{S}_j^* = \bigcup_{r \in \mathcal{D}_j} \mathcal{S}_{t_{j,r}}$.
- ii. We assign a weight w_ℓ to each partition $\tilde{\pi}_\ell$ in \mathcal{S}_j^* , with $\ell = 1, \dots, m_j$. Each weight is computed, up to a proportionality constant, by evaluating (19) at $\pi_j^* = \tilde{\pi}_\ell$.
- iii. We sample one value for π_j^* out of the m_j candidates in \mathcal{S}_j^* , with probabilities w_1, \dots, w_{m_j} .

C MORE ON THE SIMULATION STUDIES OF SECTION 4

We present additional plots related to the simulated data in Section 4.

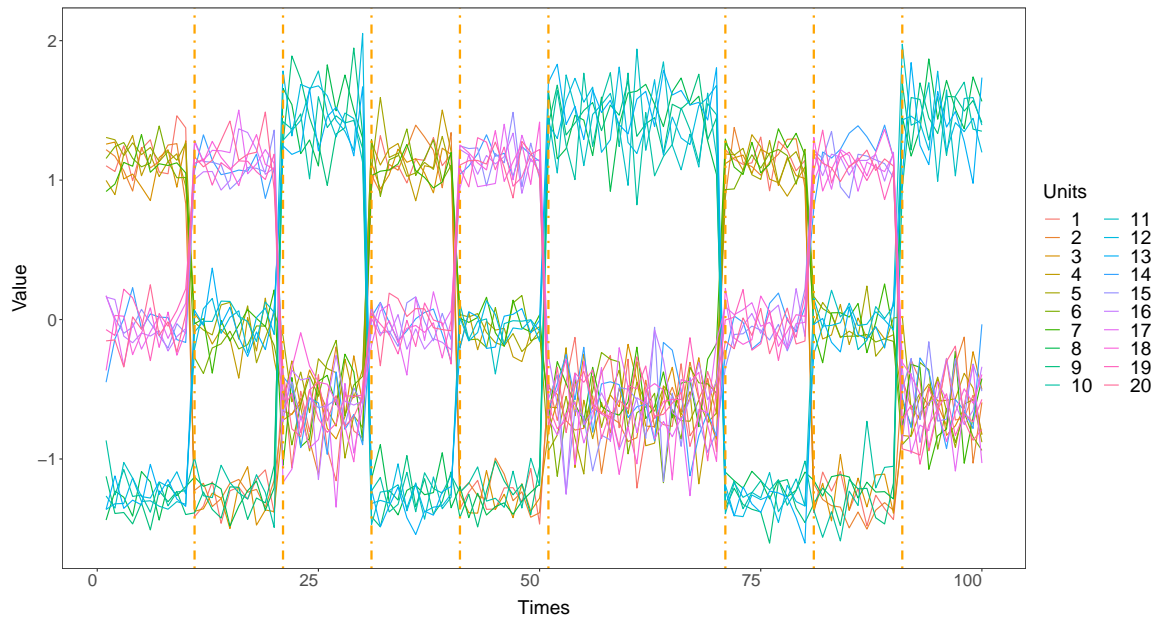


Figure C.8: Example of simulated independent dataset, with $n = 20$ subjects and $T = 100$ time points. The orange vertical lines correspond to changepoints. See Section 4.1 for details.

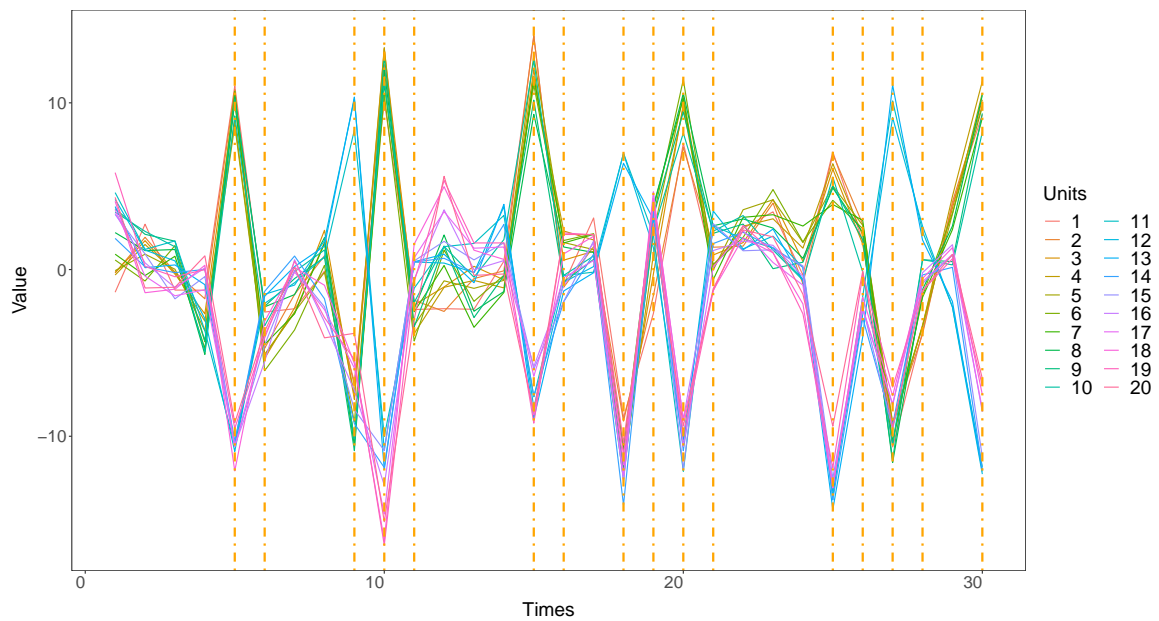


Figure C.9: Example of simulated autoregressive dataset, with $n = 20$ subjects and 30 time points. The orange vertical lines correspond to changepoints. The autoregressive coefficient is 0.9. See Section 4.2 for details.

D GESTURE PHASE SEGMENTATION

In this Section we represent additional plots referring to the application presented in Section 5.

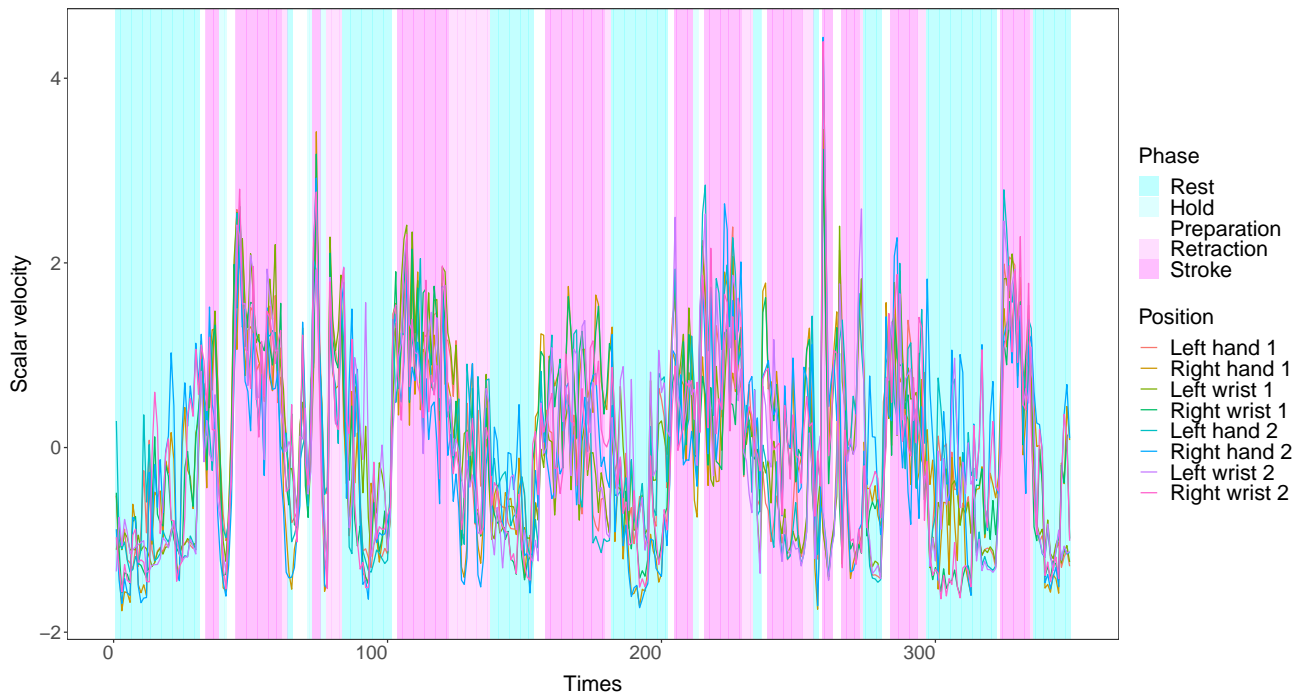


Figure D.10: Human Gesture data with the phases of the video on the background, as estimated by [Madeo et al. \(2013\)](#). See Section 5 for details.

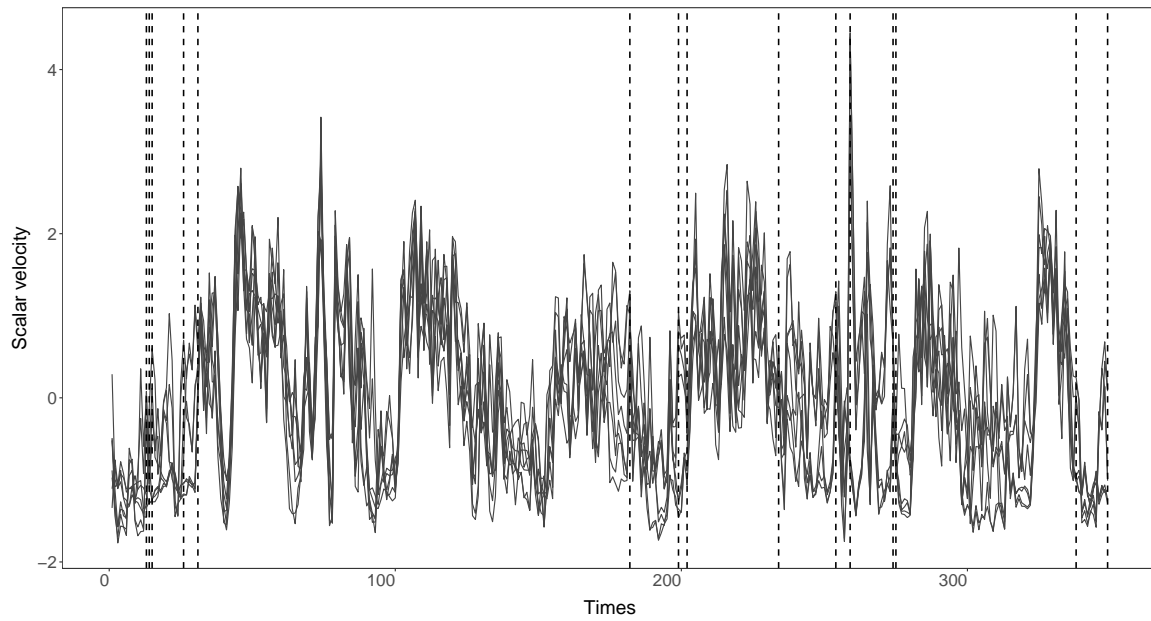


Figure D.11: Human Gesture data. Changepoints (dashed line) identified with the DRPM. See Section 5 for details.

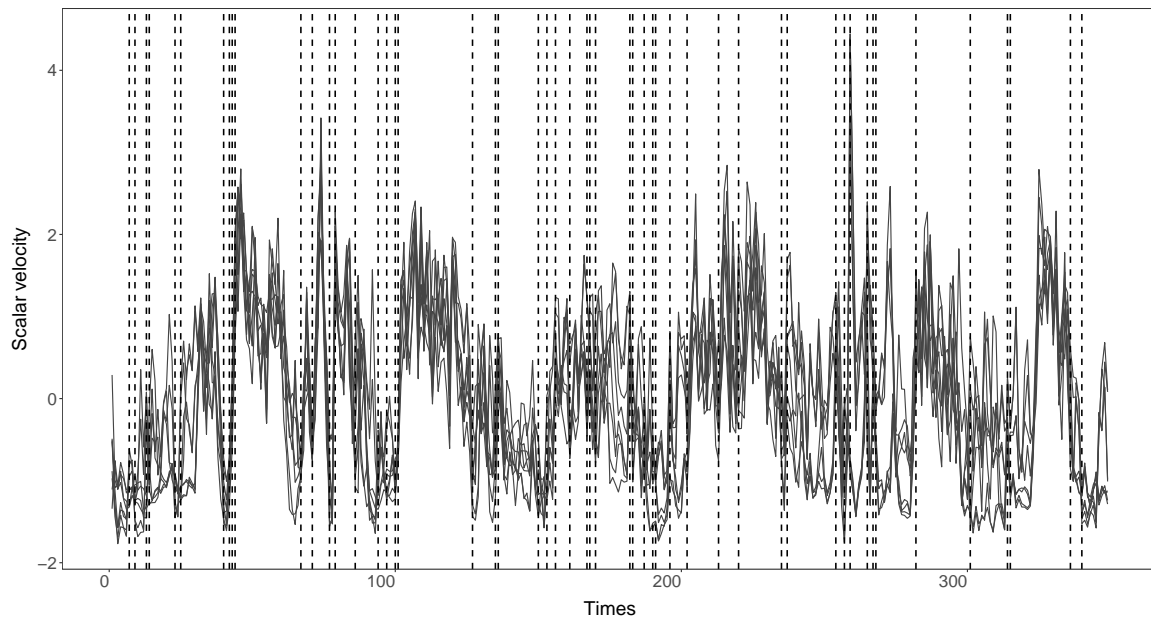


Figure D.12: Human Gesture data. Changepoints (dashed line) identified with the LDDP model. See Section 5 for details.

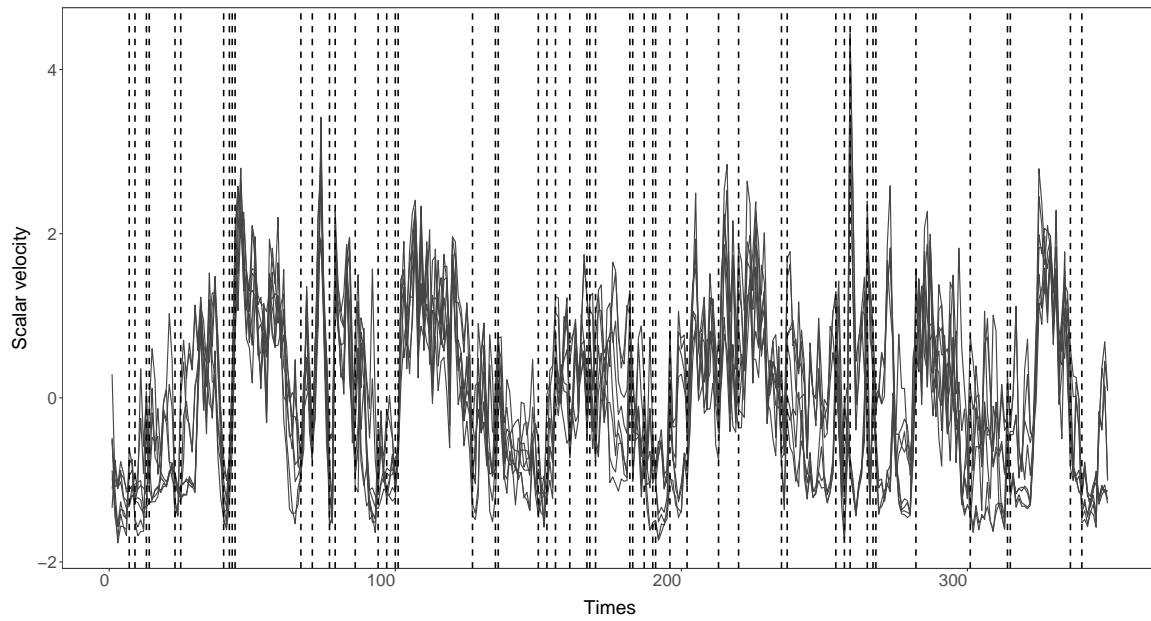


Figure D.13: Human Gesture data. Changepoints (dashed line) identified with the WDDP model. See Section 5 for details.

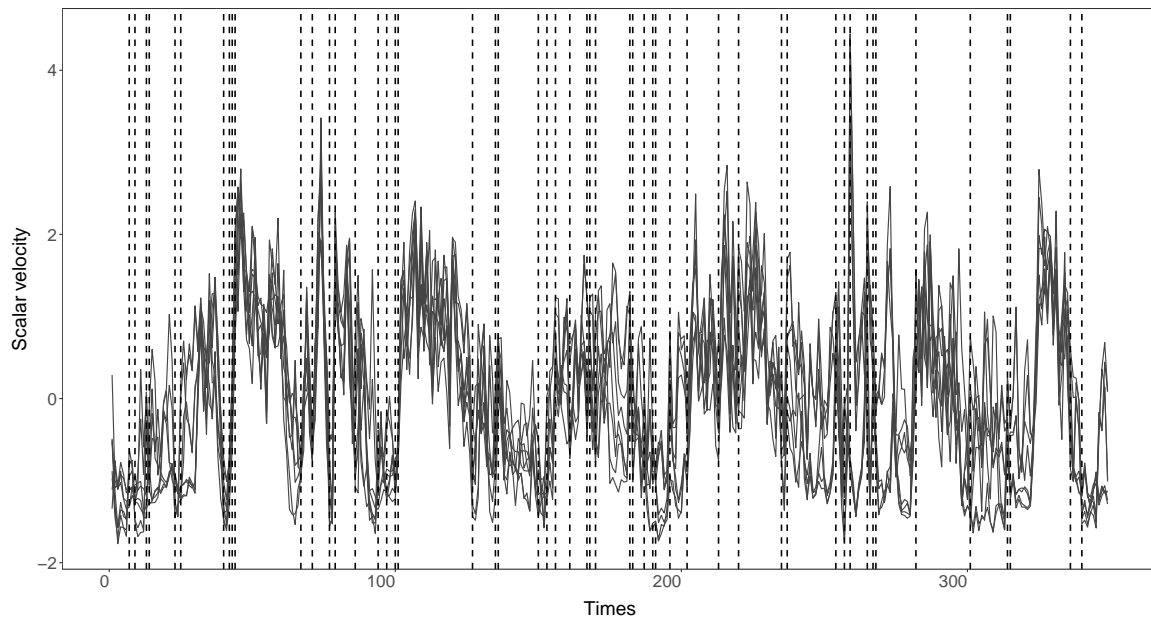


Figure D.14: Human Gesture data. Changepoints (dashed line) identified with the GMDDP model. See Section 5 for details.